frontiers | Frontiers in Astronomy and Space Sciences

TYPE Review
PUBLISHED 05 March 2025
DOI 10.3389/fspas.2024.1530392

OPEN ACCESS

EDITED BY
Jirong Mao,
Chinese Academy of Sciences (CAS), China

REVIEWED BY
Fabrizio Tavecchio,
National Institute of Astrophysics (INAF), Italy
Liyi Gu,
Netherlands Institute for Space Research (NWO), Netherlands

*CORRESPONDENCE
Sibasish Laha,
sib.laha@gmail.com,
sibasish.laha@nasa.gov

RECEIVED 18 November 2024
ACCEPTED 23 December 2024
PUBLISHED 05 March 2025

CITATION
Laha S, Ricci C, Mather JC, Behar E, Gallo L, Marin F, Mbarek R and Hankla A (2025) X-ray properties of coronal emission in radio quiet active galactic nuclei.
Front. Astron. Space Sci. 11:1530392.
doi: 10.3389/fspas.2024.1530392

X-ray properties of coronal emission in radio quiet active galactic nuclei

Sibasish Laha[1,2,3]*, Claudio Ricci[4,5], John C. Mather[1], Ehud Behar[6], Luigi Gallo[7], Frederic Marin[8], Rostom Mbarek[1,9] and Amelia Hankla[9]

[1]Astrophysics Science Division, NASA Goddard Space Flight Center, Greenbelt, MD, United States, [2]Center for Space Science and Technology, University of Maryland Baltimore County, Baltimore, MD, United States, [3]Center for Research and Exploration in Space Science and Technology, NASA/GSFC, Greenbelt, MD, United States, [4]Instituto de Estudios Astrofísicos, Facultad de Ingeniería y Ciencias, Universidad Diego Portales, Santiago, Chile, [5]Kavli Institute for Astronomy and Astrophysics, Peking University, Beijing, China, [6]Department of Physics, Technion, Haifa, Israel, [7]Department of Astronomy and Physics, Saint Mary's University, Halifax, NS, Canada, [8]Université de Strasbourg, CNRS, Observatoire Astronomique de Strasbourg, Strasbourg, France, [9]Department of Astronomy, University of Maryland, College Park, MD, United States

Active galactic nuclei (AGN) are powerful sources of panchromatic radiation. All AGN emit in X-rays, contributing around 5%–10% of the AGN bolometric luminosity. The X-ray emitting region, popularly known as the corona, is geometrically and radiatively compact with a size typically $\lesssim 10\ R_G$ (gravitational radii). The rapid and extreme variability in X-rays also suggest that the corona must be a dynamic structure. Decades of X-ray studies have shed much light on the topic, but the nature and origin of AGN corona are still not clearly understood. This is mostly due to the complexities involved in several physical processes at play in the high-gravity, high-density and high-temperature region in the vicinity of the supermassive black hole (SMBH). It is still not clear how exactly the corona is energetically and physically sustained near a SMBH. The ubiquity of coronal emission in AGN points to their fundamental role in black hole accretion processes. In this review we discuss the X-ray observational properties of corona in radio quiet AGN.

KEYWORDS

active - galaxies, black hole - X-rays, corona, supermassive black hole, galaxies - active

1 Introduction

Some of the most energetic emission in an active galactic nucleus (AGN) hosting an accreting supermassive black hole (SMBH) is produced in the X-rays. The AGN corona which is responsible for most of the X-ray emission, is an extremely hot ($T \sim 10^9$K) plasma residing very close to the SMBH. The coronal X-ray spectrum is a power-law in the energy range ~0.3 – 100 keV (Vaiana and Rosner, 1978; Haardt and Maraschi, 1993; Merloni et al., 2003), and contributes to around 5 – 10% of AGN bolometric luminosity (Elvis et al., 1994; Marconi et al., 2004; Vasudevan and Fabian, 2007; Fabian et al., 2017). Over the past 40–50 years of X-ray observations, important discoveries have been made in AGN coronal physics, which have opened up new fundamental questions, such as: 1) What is the structure and extent of the corona, and how is it sustained in the high gravity regime? 2) What determines the fraction of thermal and non-thermal electron components in the

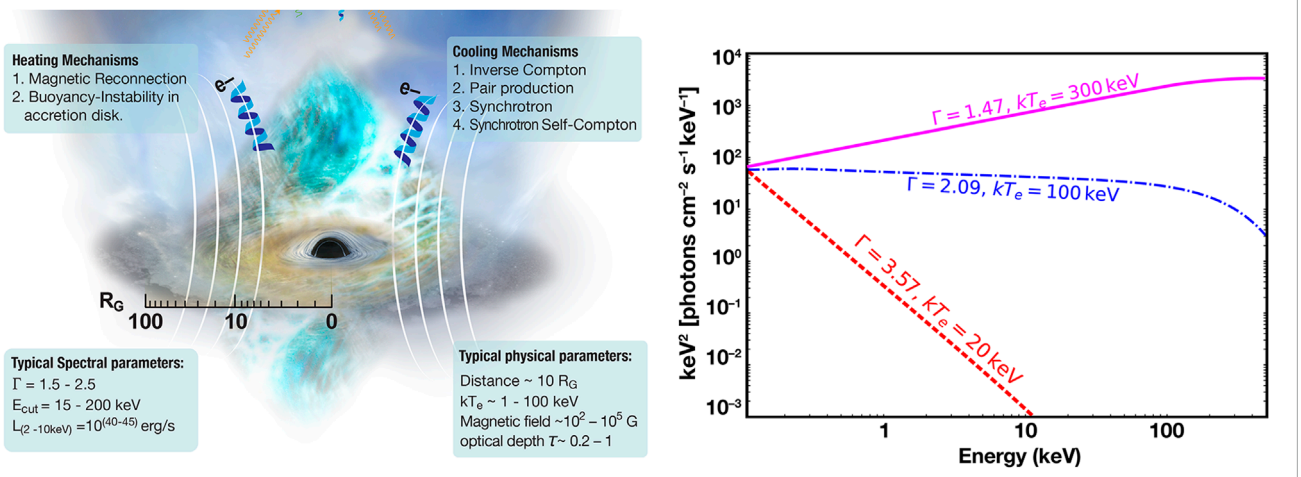

FIGURE 1
AGN coronal typical parameters and spectra. Left Panel: A cartoon of an AGN central engine with the SMBH (black), accretion disk (brown), the X-ray emitting corona (diffuse cyan), the larger scale outflows (blue) and typical electron orbits around the magnetic fields (helical strips). R_G refers to the gravitational radius of the SMBH. The magnetic field lines are shown in white. *Top left and right:* dominant heating and cooling mechanisms (see for, e.g., Done and Fabian, 1989; Balbus and Hawley, 1998; Di Matteo, 1998; Miller and Stone, 2000; Fabian et al., 2015, and references therein). *Lower left:* the typical ranges in the spectral parameters: X-ray power law slope (Γ), power law cut-off energy (E_{cut}) and 2 – 10 keV luminosity ($L_{2-10\,keV}$). *Lower right:* typical ranges in the coronal physical parameters: Distance from the SMBH, electron temperature (kT_e), Magnetic field in Gauss, and X-ray optical depth (τ). See for, e.g., Ricci et al. (2017), Ricci et al. (2018); Kamraj et al. (2022). The typical spectral and physical parameter ranges quoted here represent the bulk of the Radio-Quiet AGN population, though values beyond these ranges are also detected in some AGN. We also note that the lower limit on AGN X-ray luminosity quoted here corresponds to the detection threshold of current generation instruments and not an intrinsic AGN limit. Right panel: The shape of the power law continuum for different coronal electron temperatures (for a full discussion see Ricci et al., 2018). We used the COMPPS model in XSPEC (Arnaud, 1996) to simulate Comptonization spectra in X-ray corona. We assumed the following: (a) A spherical geometry of the corona, (b) the plasma optical depth $\tau = 0.8$, (c) the disk (UV) seed photons having a temperature of 10eV. We normalized the three spectra at 0.1 keV. The resulting slope of the power law spectra are reported. We note that with increasing electron temperature the spectral slope becomes harder.

corona? 3) How is energy pumped and dissipated in the corona? Is the corona in radiative equilibrium?

The central engine of AGN (see Figure 1 left panel) is thought to consist of an accretion disk surrounding the SMBH. The loss of gravitational energy of the accreting material is expected to be one of the main sources of the energy in AGN, part of which is manifested in the optical and UV bands (Shakura and Sunyaev, 1973). The rate at which the system is accreting is often parametrized as the Eddington ratio (λ_{Edd})[1].

In this review we will focus on the coronal X-ray emission from radio quiet AGN (RQ-AGN), which represent the largest population of accreting SMBHs. We do not discuss radio loud AGN (RL-AGN) in this review because the jets may contribute to the X-rays adding extra complexities and contaminate X-ray emission from the corona. We note that in a short review of a mature field such as AGN coronal emission, it is not possible to cover all topics related to the subject, and some subjectivity may unintentionally introduce bias.

This manuscript is arranged as follows: In Section 1.1 we discuss some of the most important physical processes in AGN coronae. In Section 2 we list the phenomenology of the coronal emission discussing the most relevant discoveries and the empirical relations between X-ray coronal emission and the other observable quantities. In Section 3 we briefly address some of the open questions in the field, and in Section 4 we discuss future perspectives.

1.1 The primary physical processes in AGN corona

The coronal X-ray emission can be simply characterized by a power law with a photon index (Γ) and cut-off energy (E_C), such that the flux $F(E) \propto E^{-\Gamma} e^{-E/E_C}$. Some of the main observables of X-ray coronae that can be inferred from X-ray spectroscopy are: (1) the spectral slope Γ, which is related to the temperature of the Comptonizing electrons (kT_e) and the optical depth (τ) of the X-ray emitting plasma (Rybicki and Lightman, 1979), (2) the high energy cut-off E_C and (3) the X-ray luminosity $L_{0.3-100\,keV}$. We briefly discuss some of the most important physical processes that are expected to take place in AGN coronae, and we refer the readers to Rybicki and Lightman (1979) for a detailed exposition.

1.1.1 Inverse compton scattering

Inverse Compton (IC) scattering is thought to be the dominant process responsible for X-ray emission in AGN. When UV seed photons from the accretion disk, with energies $h\nu$, pass through the coronal plasma, energy gets transferred from the hot (10^9 K) electrons to the photon field by repeated IC scattering. This happens if $h\nu < 4kT_e$, where h is the Planck constant, ν is the photon frequency, k is the Boltzmann constant and T_e is the temperature of the electrons.

For a plasma of non-relativistic electrons in thermal equilibrium with energy $kT_e \ll m_e c^2$, having an optical depth τ_{es}, one can define the Compton y parameter: $y = \max(\tau_{es}, \tau_{es}^2)(4kT_e/m_e c^2)$, where m_e is the electron mass and c is the speed of light. For $y \gg 1$, the

1 $\lambda_{Edd} = L_{bol}/L_{Edd}$, where L_{bol} is the bolometric luminosity and L_{Edd} is the Eddington luminosity.

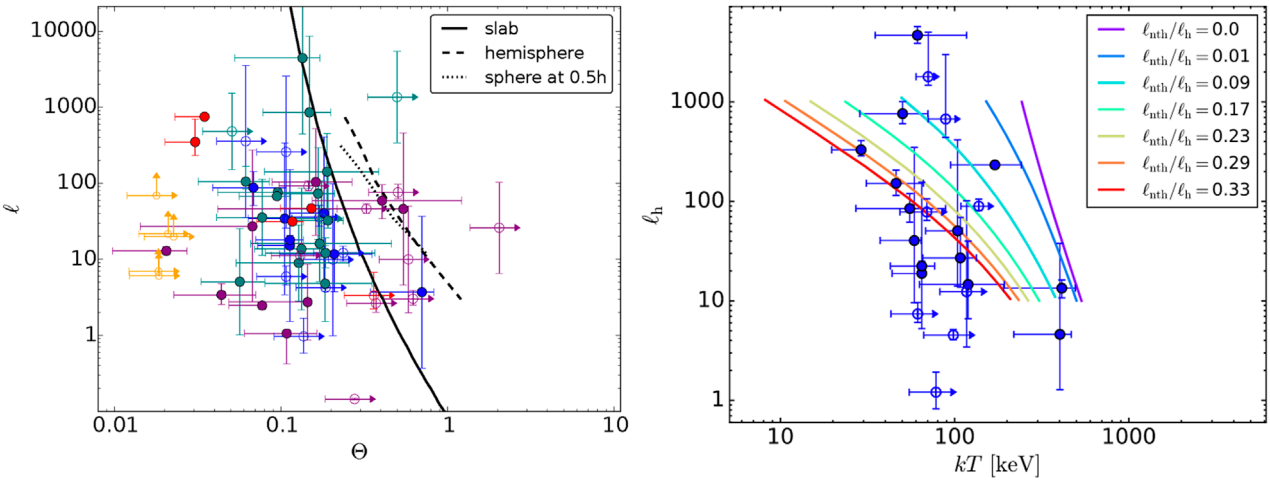

FIGURE 2
Pair production acting as a thermostat for coronal plasmas. Left: Compactness parameter (l) and temperature (Θ) phase space plotted for AGN that have measured cut-off energies in the X-ray band (Fabian et al., 2015; 2017). The black, dashed and dotted lines are theoretical curves denoting the limits for the pair production process for a slab, hemisphere and spherical geometries, respectively. Right: Same as left, but now the different colored curves denote varying contributions from thermal and non-thermal plasmas, with the non-thermal fraction increasing from right (purple curve) to left (red curve). Figure reproduced by permission of Oxford University Press on behalf of the Royal Astronomical Society.

average photon energy reaches the thermal energy of the electrons and is called 'saturated inverse Compton scattering'. The case for unsaturated Comptonization ($y > 1$) is however of most interest in black hole systems, and in such a case, the output spectrum in the X-ray is a power law with a high energy cut-off $E_{\rm C}$ determined by the electron temperature, which is typically approximated to be $E_{\rm C} \sim 2-3kT_{\rm e}$ (Petrucci et al., 2001; Fabian et al., 2015).

1.1.2 Synchrotron emission

The high densities of electrons around the magnetic field in AGN corona makes it a significant synchrotron emitter predominantly between 5 – 200 GHz (Laor and Behar, 2008; Panessa et al., 2019; Baldi et al., 2022; Kawamuro et al., 2022; Ricci et al., 2023). The fact that we see 1) ubiquitous unresolved mm emission even with high spatial resolution, 2) flat radio slopes, and 3) strong correlation between the radio and X-rays in RQ-AGN are indicators of radio emission from the corona through synchrotron processes (Panessa et al., 2019). For example, recent results (Ricci et al., 2023) point toward a tight correlation between 2 – 10 keV and 100 GHz luminosity for a volume-limited sample of nearby hard X-ray selected RQ-AGN. Similarly, the core radio flux at 5 GHz and the 2 – 10 keV luminosity for nearby radio quiet AGN have been found to show an interesting correlation $L_{\rm R,5GHz}/L_{2-10\,\rm keV} \sim 10^{-5.5}$ (Laor and Behar, 2008) which is similar to that found in coronally active stars (such as the Sun) and is popularly known as the Gudel-Benz relation (Guedel and Benz, 1993). As a caveat we note here that the coronal magnetic field can be as high as $B = 10^2 - 10^5$ Gauss and significant synchrotron self absorption (SSA) effects may limit our detection at lower frequencies (below ~40 GHz).

Direct measurement of magnetic fields in AGN corona has not yet been possible, but we can estimate a typical range from the analogy of RL-AGN. Large B_0 values on event horizon scales are feasible considering that measurements from AGN jets have previously found magnetic field strengths of ~0.1 G on ~1 pc scales from core frequency-shift methods (O'Sullivan and Gabuzda, 2009) and ~10 G on ~0.1 pc scales from Faraday rotation measurements (Martí-Vidal et al., 2015). Such observational values are consistent with $B_0 \gtrsim 10^5$ G at the base of the jet with a $1/r$ decay of the magnetic field, and are thereby consistent with theoretical and numerical predictions for launching relativistic jets (Tchekhovskoy et al., 2011).

1.1.3 Electron-positron pair production

Sources which are physically compact and highly luminous, like the AGN corona, are also radiatively compact. This means that the photons and the particles in the plasma are in constant interaction with each other. In such a plasma, photon–photon collisions can lead to $e^- - e^+$ pair production, when the photons are energetic enough. The resulting $e^- - e^+$ pair density is proportional to the luminosity (L) and electron temperature (kT_e or $\Theta = kT_e/m_ec^2$), and inversely proportional to the source size (R) assuming a spherical source. This is typically expressed by the compactness parameter $l = L\sigma_{\rm T}/(Rm_ec^3)$ where $\sigma_{\rm T}$ is the Thomson cross-section. Thus, when the energy content of corona increases, manifested by an increase in both l and $kT_{\rm e}$, the extra energy goes into creating more pairs, rather than increasing the temperature. Therefore, the process acts as a natural thermostat for the corona (Done and Fabian, 1989; Fabian et al., 2015; 2017). See Figure 2 left panel.

If magnetic reconnection is a dominant form of energy production mechanism in the X-ray corona (Di Matteo, 1998), then one would expect a fraction of non-thermal electrons (Done and Fabian, 1989). The existence of non-thermal particles in the corona would result in a distribution of photon energy that extends into the MeV band. This small number of high energy particles could be highly effective in seeding pair production. Moreover, the cooled non-thermal pairs could share the total available energy, thus reducing the mean energy per particle and therefore decreasing the temperature of the thermal population. Such hybrid coronal plasma,

consisting of thermal and non-thermal electron populations, might have been found in a few nearby AGN (See Figure 2 right panel), in which the Comptonizing plasma is found well below the pair production line in the $l - kT_e$ plane (Fabian et al., 2015; 2017).

2 Phenomenological properties of the corona

X-ray emission from AGN was detected and studied already by the early X-ray observatories such as *Ariel-V* (1974–1980, Smith and Courtier, 1976), *HEAO-1* (1977–1983, Rothschild et al., 1979), *HEAO-2* or *Einstein* (1978–1981, Giacconi et al., 1979), *EXOSAT* (1983–1986, Taylor et al., 1981), *GINGA* (1987–1991, Makino and ASTRO-C Team, 1987). In the later period *ASCA* (1993–2001, Tanaka et al., 1994) and *RXTE* (1995–2012, Swank, 1999) provided seminal insights into the X-ray properties of the AGN corona. For example, the ubiquity of X-ray emission from Seyfert-1 galaxies was established (Elvis et al., 1978) by the first catalog from the Ariel-V sky survey (Cooke et al., 1978). The first large spectral samples of AGN observed by HEAO-1 revealed that the observed range in photon spectral indices was tightly distributed around $\Gamma \approx 1.7$ (Mushotzky et al., 1980; Rothschild et al., 1983; Mushotzky, 1984). The *Einstein* and *EXOSAT* missions demonstrated that rapid, large amplitude X-ray variability is a common feature in nearby AGN, and that such variability is stochastic and it shows no characteristic timescale (Lawrence et al., 1987; McHardy and Czerny, 1987).

These discoveries were followed by the era of the great X-ray observatories, which started with the launch of *Chandra* (1999-, Weisskopf et al., 1996) and *XMM-Newton* (1999-, Lumb et al., 2012), and later with the advent of hard X-ray (>10 keV) observatories such as *INTEGRAL* (2002-, Winkler et al., 2003), *Swift*-BAT (2004-, Barthelmy et al., 2005), *Suzaku* (2005–2015, Mitsuda et al., 2007) and *NuSTAR* (2012-, Harrison et al., 2013). Our understanding of AGN corona over the years has improved significantly, but much remains to be understood. In this section, we will review some of the most important observational characteristics of AGN coronal emission obtained with the above mentioned observatories.

2.1 The coronal plasma spectral and physical properties

2.1.1 Coronal X-ray power law slope and optical depth

Figure 1 left panel highlights the primary spectral and physical characteristics of X-ray coronae and their typical range of values. The left panel of Figure 3 shows the photon index (Γ) distribution for a large sample of AGN (both obscured and unobscured) studied with broad-band X-ray observations (0.3–150 keV), with a median value of 1.78 ± 0.1 (Ricci et al., 2017). Recent broad-band X-ray studies also show that the spectral slope of the 14 – 195 keV emission is steeper than the 0.3 – 10 keV band, suggesting the high energy cut-off is ubiquitous in AGNs (Ricci et al., 2017).

The photon index is dependent on both the plasma temperature and the optical depth, and it can be estimated as $\Gamma \sim [\frac{9}{4} + \frac{m_e c^2}{kT_e \tau(1+\tau/3)}]^{0.5} - \frac{1}{2}$ (Rybicki and Lightman, 1979). By measuring both Γ and E_C it is possible to estimate the optical depth of the Comptonizing plasma, assuming a geometry (see, for example, Brenneman et al., 2014). Recent studies of nearby AGN estimate a median value of the optical depth of $\tau = 0.25 \pm 0.06$ (Ricci et al., 2017).

2.1.2 Coronal luminosity and bolometric correction

The typical coronal luminosity can span a large range $L_{2-10\,\mathrm{keV}} \sim 10^{40-45}\,\mathrm{erg\,s^{-1}}$ (Piconcelli et al., 2005; She et al., 2017; Ricci et al., 2017), with the lower limit being only loosely defined by detector sensitivity and increasing contribution of non-AGN process to the X-ray emission. On this low-luminosity end of the distribution are the sources that are either accreting at low Eddington ratios or host intermediate mass black holes ($\log(M_{BH}/M_\odot) < 6$, Dong et al., 2012). On the extreme high-luminosity end, are the hyperluminous AGN with $L_{2-10\,\mathrm{keV}} \geq 10^{45}\,\mathrm{erg\,s^{-1}}$, typically found at $z \sim 2-4$ encompassing the cosmic peak of quasar activity (Martocchia et al., 2017).

The contribution of the X-rays to the total AGN emission is usually parametrized with the X-ray bolometric correction (κ_{2-10}): $\kappa_{2-10} \sim L_{bol}/L_{2-10\,\mathrm{keV}}$. Studies of nearby AGN have shown that more luminous sources typically have weaker coronal X-ray emission relative to their bolometric luminosity, with $\kappa_{2-10} \simeq 15-25$ at $\lambda_{Edd} < 0.1$, and $\kappa \sim 40-70$ at $\lambda_{Edd} > 0.1$ (Vasudevan and Fabian, 2007).

2.1.3 The high energy cut-off (E_C) and the coronal temperature

The high energy cut-off of the power law component is related to the coronal temperature as $E_C \sim 2kT_e$, for an optically thin plasma, i.e., $\tau \lesssim 1$. On the other hand when the plasma is optically thick, i.e., $\tau \gg 1$ the relation is $E_C \sim 3kT_e$, both approximated for a corona of slab geometry (Petrucci et al., 2000; 2001). The right panel of Figure 3 (Kamraj et al., 2022) shows the distribution of high-energy cut-offs inferred from *NuSTAR* observations of a sample of nearby AGN. The median value of the cut off energy obtained for the sample is ~84 ± 9 keV. A large study of a sample of nearby *Swift*-BAT detected AGN finds a median cut-off energy in local AGN that is significantly higher ($E_C \sim 200 \pm 29$ keV; Ricci et al., 2017). Indirect constraints on the cut-off energy have been obtained by fitting the cosmic X-ray background (CXB), and have shown that the mean cut-off energy is likely below 300 keV(Gilli et al., 2007; Treister et al., 2009; Ueda et al., 2014), in agreement with the observational studies reported above.

Analyzing a sample of ~200 AGN, Ricci et al. (2018) found that, while E_{cut} is not related to the mass of the black hole or the 14 – 150 keV luminosity, it appears to be related to the Eddington ratio (λ_{Edd}). Sources with $\lambda_{Edd} > 0.1$ were shown to display significantly lower median cut-off energy ($E_{cut} = 160 \pm 41$ keV) than those with $\lambda_{Edd} \leq 0.1$ ($E_{cut} = 370 \pm 51$ keV). This supports the idea that more radiatively compact coronae are cooler, because they tend to avoid the region in the temperature-compactness parameter space where runaway pair production would dominate (See Figure 2). In some extreme cases, coronal temperatures as low as $kT \sim 10-20$ keV have been measured in a few nearby AGN (Buisson et al., 2018). Interestingly, and in agreement with the results of Ricci et al. (2018), such cool corona are often detected in several high Eddington AGN (Kara et al., 2017; Tortosa et al., 2022). These plasma are either not

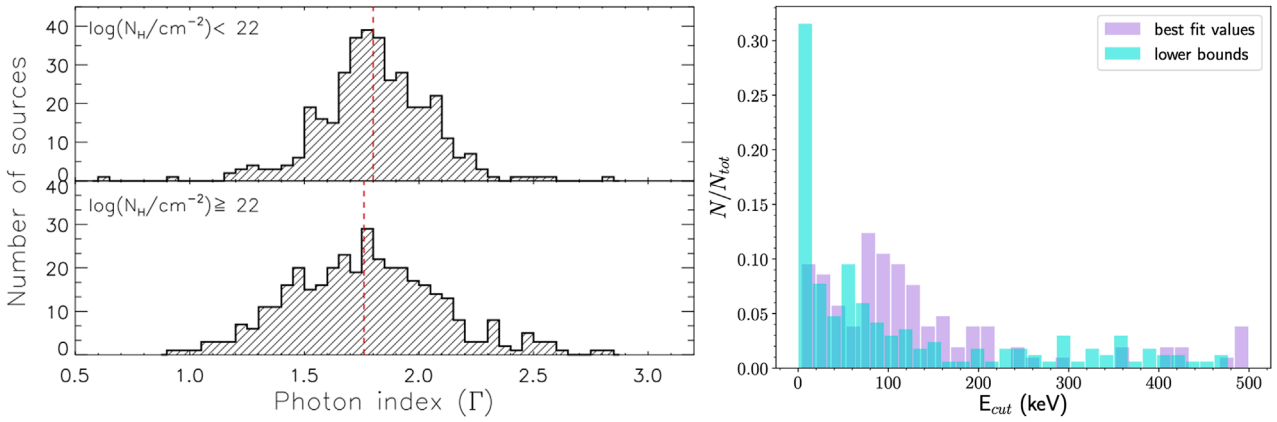

FIGURE 3
Distribution of the X-ray spectral parameters of AGN coronal emission: Left: The distribution of the photon-indices Γ for X-ray unobscured (top panel) and X-ray obscured (lower panel) sources (Ricci et al., 2017). Right: Distribution of the cut-off energy as measured for a sample of AGN with *NuSTAR* hard X-ray observations (Kamraj et al., 2022), when the spectra are modeled using a simple absorbed power law. The cyan and purple histograms represent the lower bounds and the best-fit values, respectively. Both panels reproduced with permission © AAS.

pair-production dominated, or they are hybrid, as discussed in the Introduction.

Sample studies of AGN in hard X-rays with *NuSTAR* detected an anti-correlation between kT_e and τ (Tortosa et al., 2018; Kamraj et al., 2022; Serafinelli et al., 2024). On average, the lower mass, highly accreting narrow line Seyfert 1 galaxies (NLSy1s) exhibit a steeper photon index ($\Gamma > 2$), suggesting the corona might be cooler or less optically thick compared to other AGN (e.g., Brandt et al., 1997; Gallo, 2018).

2.2 The coronal size, geometry and stability

Although corona is known to be compact (Ghisellini et al., 2004; Fabian et al., 2015), it can sometimes be patchy (e.g., Haardt and Maraschi, 1991; Stern et al., 1995; Petrucci et al., 2013; Wilkins and Gallo, 2015c). Four (simplified) coronal geometries that are commonly discussed in the literature: a point source, a cylindrical slab, a spheroid/ellipsoid, and a conical geometry (Gonzalez et al., 2017). Ray-tracing simulations suggest that some of these geometries could be distinguished through X-ray spectral modelling (e.g., Wilkins and Fabian, 2012; Dauser et al., 2013; Gonzalez et al., 2017) and polarization studies (e.g., Schnittman and Krolik, 2010; Zhang et al., 2019).

Although the geometry of the corona is extremely hard to determine, the size of the corona can be inferred from several indirect methods:

2.2.1 Spectral and spectral-timing techniques

2.2.1.1 Emissivity profile

The emissivity profile describes the amount of reprocessed radiation emitted from the disc as a function of distance from the illuminating source, and it is typically inferred from the properties of the relativistically broadened emission lines (e.g., Fe Kα). The emissivity profile is dependent on the morphology of the corona and its height above the disc (e.g., Wilkins and Fabian, 2011; 2012; Dauser et al., 2013; Gonzalez et al., 2017). Measurements of the emissivity profile in a few well studied AGN suggest that the corona is relatively compact ($\lesssim 10 R_G$, Wilkins et al., 2014; Wilkins and Gallo, 2015a).

2.2.1.2 Reflection fraction

The detection of broad (and redshifted) FeKα emission lines and its variability in some sources clearly indicates the presence of general relativistic effects in producing the line shape, which may arise out of reflection from the inner regions of an accretion disc (Miniutti and Fabian, 2004). The ratio of the reflected flux (primary flux reflecting off the disk) and the primary X-ray flux can provide some constraints on the location and motion of the corona (Wilkins and Gallo, 2015b; Dauser et al., 2016; Gonzalez et al., 2017). For example, a detailed spectral analysis of the low-flux state of Mrk 335 by *NuSTAR* revealed a spectra with a high reflection fraction (>8) indicating relativistically blurred emission, from a X-ray point source (corona) collapsing down to within $\sim 2R_G$ of the SMBH event horizon. Later on with increasing X-ray flux, the reflection fraction decreased, consistent with a corona moving up to $10\,R_G$ as the source brightened (Parker et al., 2014).

2.2.1.3 X-ray variability

Coronal X-ray emission shows variability at different time scales (δt), from a few 100 s to days (McHardy et al., 2005; Middei et al., 2022; Reeves et al., 2021). The shortest variability timescales put an upper limit to the size of the emitting region $R < c\delta t \simeq 1 - 10\,R_G$. Variability in the coronal emission is echoed in the emission reflected in the accretion disc, with some delay that corresponds to the light travel time between the corona and the disk (e.g., Fabian et al., 2009; Zoghbi et al., 2010; Uttley et al., 2014). These reverberation lags can provide insights on the location of the corona relative to the inner disc. For sources where reverberation lags have been detected, indications are that the region is compact and typically less than $\sim 10 R_G$ (De Marco et al., 2013;

Kara et al., 2016; Wilkins and Fabian, 2013; Cackett et al., 2014; Kara et al., 2013; Zoghbi et al., 2012).

2.2.2 X-ray polarization

Compton scattering induces polarization of the X-ray photons, which is an important tool to study the geometry of the emitting plasma. The polarization of the X-ray photons measured both in degree and position angle, is energy- and geometry dependent. For example, a polarization degree of 4% or higher can possibly rule out spherical and lamp-post coronal models, because symmetry reduces the polarization degree (Zhang et al., 2019; Ursini et al., 2022a). The same is true for the orientation of the polarization angle, that is model-specific (different models predict different values of polarization angle).

Launched in December 2021, the Imaging X-ray Polarimetry Explorer (IXPE), is the first X-ray spectro-imaging polarimeter satellite sensitive in the 2–8 keV band (Weisskopf et al., 2022). IXPE successfully measured a polarized signature in NGC 4151 (Gianolli et al., 2023) with a polarization degree of 4.9% ± 1.1% at a position angle of 86° ± 7° east of north at 68% confidence level. The amount of polarization associated with the corona is of the order of 4%–8%, which directly excludes a spherical geometry (Beheshtipour et al., 2017; Ursini et al., 2022b). The polarization angle measured for this source, which is parallel to its radio jet, suggests that the corona could be distributed along the accretion disk or perhaps it's a part of the inner accretion flow (as in a slab geometry). On the other hand, upper limits (at 99% confidence level) of 3.2% and 6.2% were obtained for the polarization degree in MCG−5 − 23−16 (Marinucci et al., 2022a; Tagliacozzo et al., 2023) and IC 4329A (Ingram et al., 2023), respectively, implying that, for those two objects, we cannot directly rule out a spherical and/or lamppost corona. However, the orientation of the polarization angle in those two AGN seems to be more consistent with an extended corona (along the equatorial plane) rather than with a polar or spherical corona, because their tentatively measured polarization angle (at $<3\sigma$) are also parallel to the detected radio structures and polar winds (Tagliacozzo et al., 2023; Ingram et al., 2023).

Here we also mention an interesting result from an X-ray binary, Cygnus X-1, for which the polarization degree could be constrained exceptionally well, at (4.0 ± 0.2)% between 2–8 keV, and a polarization angle parallel to the jet axis (Krawczynski et al., 2022). This suggests that, similar to AGNs, the hot X-ray corona is likely spatially extended in a plane perpendicular to the jet axis, parallel to the inner accretion flow, and rules out the commonly used lamp-post model.

2.2.3 Microlensing studies

Gravitational microlensing of quasar light by a foreground mass (lens) can be used to probe the sizes related to the accretion disc and corona (e.g., Chartas et al., 2009; Morgan et al., 2008; Dai et al., 2010). Using such methods, the size of the X-ray emitting region (the corona) is estimated to be very compact, around $5-10\,R_G$ (e.g., Dai et al., 2010).

2.2.4 X-ray eclipses

Capturing the transit of the X-ray source by an obscuring cloud is fortuitous, but not rare (see for, e.g., Risaliti et al., 2007; Turner et al., 2018; Gallo et al., 2021; Ricci and Trakhtenbrot, 2022). Such events are important as they can be used to constrain the sizes of the X-ray region based on the duration of the eclipse. This method assumes that the cloud is gravitationally bound to the central SMBH in a Keplerian orbit and the eclipse occurs when the cloud moves across our line of sight to the central engine. In the objects for which eclipses could be used to measure the size of the corona (e.g., Risaliti et al., 2011; Gallo et al., 2021), the results have been consistent with those obtained using other methods.

2.3 Coronal X-ray variability and flares

AGN coronal X-ray emission is variable at different timescales and with different amplitudes (see for, e.g., McHardy and Czerny, 1987; Mushotzky et al., 1993; Papadakis, 2004; McHardy et al., 2004; 2006; Serafinelli et al., 2024, and references therein). Here we briefly discuss three types of AGN X-ray coronal variability commonly observed: (a) Stochastic variability, (b) quasi-periodic variability and (c) Flares, and we note that a detailed discussion of timing and spectral-timing studies of AGN corona is beyond the scope of this short review.

2.3.1 Stochastic variability

One of the most common coronal variability pattern is the chaotic total intensity variation, or stochastic variation. Early studies using observations from Ariel-V and EXOSAT show that 40% of AGN exhibit stochastic variability on a timescale less than 1 day, and 97% of them showed variability on longer timescales (e.g., Grandi et al., 1992; McHardy and Czerny, 1987). More recently, a linear relationship between the rms amplitude of short-term variability and flux variations on longer timescales has been found in AGN X-ray light curves (Gaskell, 2004; Uttley et al., 2005a; Vaughan et al., 2011). This has been dubbed the "rms-flux" relation (Uttley et al., 2005b). This is an important feature of the aperiodic variability of accreting compact objects, including black hole X-ray binaries (Gleissner et al., 2004; Heil et al., 2012).

It is still unclear how the X-ray coronal variability at different-timescales is produced. Popular models predict that inward propagation of random accretion rate fluctuations in the accretion flow could create such stochastic variations in the coronal X-ray emission (Lyubarskii, 1997; Kotov et al., 2001; King et al., 2004; Kelly et al., 2011; Ingram and van der Klis, 2013; Cowperthwaite and Reynolds, 2014). The longer term variability may be produced by accretion rate changes (Mushotzky et al., 1993), but the origin of the short timescale variations (a few ks or less) are still debated. The magnetic field reconnection in accretion disk threading the coronal plasma likely play a role (Di Matteo, 1998) as they do in the solar corona.

An important measurement of the variability is the power density spectrum (van der Klis, 1989; Vaughan et al., 2003a; b), which describes the amount of power (the amplitude squared, i.e., the power of the signal) as a function of temporal frequency. When the X-ray light curve can be described as random displacements around a mean value, then the power density spectrum (PSD) shows a constant value, that is, all frequencies have equal power. This is known as a white noise spectrum. On the other hand, a red noise spectrum is created when the points in the light curve have

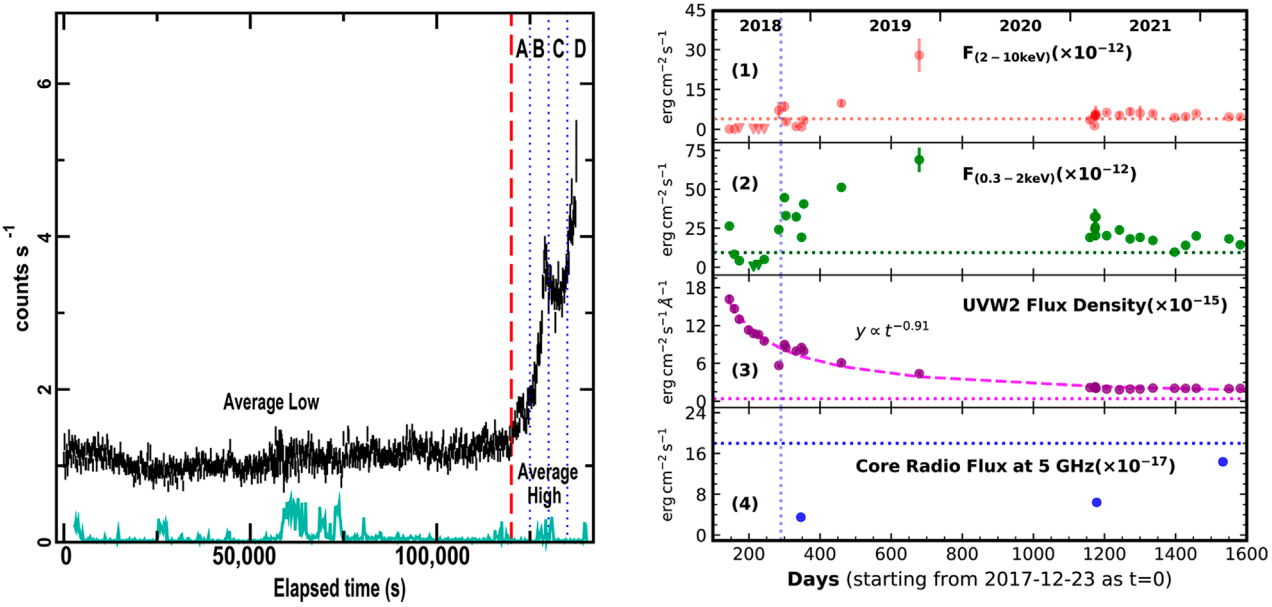

FIGURE 4
The short and long term X-ray flares in AGN corona. Left: The short term ($\lesssim$100ks) X-ray flare in the type-1 AGN Mrk 335 captured by *XMM-Newton* during the rise (Gallo et al., 2019). The flux increased by a factor of ~5 in 20ks. The 2 – 10 keV coronal spectral slope Γ show gradual softening during the flare-rise (soft-when-bright behavior), estimated for the time bins A, B, C and D (Gallo et al., 2019). The black curve is the source + background light curve, while the cyan curve is the background light curve. *Right:* The long term X-ray, UV and radio light curve of the changing-look AGN 1ES 1927 + 654 spanning 4 years (2018–2022). From top to bottom are: (1) X-ray 2 – 10 keV flux, (2) X-ray 0.3 – 2 keV flux, (3) The UVW2 flux, (4) The core radio (< 1pc) flux at 5GHz. The top three panels are from *Swift* observatory, while the radio data are from VLBA. While both the soft and the hard X-rays first vanished and then flared by a factor of ~10 in 1 year, the UV showed a constant decline with a power law fall ($\propto t^{-0.91}$) indicating no correlation between the X-rays and the UV. The core radio flux was at its lowest when the X-rays were at its lowest state indicating a close connection between these two bands (Laha et al., 2022; Ghosh et al., 2023). The vertical dotted line denotes the time when the X-rays revived. The horizontal lines in every panel refer to the pre-changing-look values obtained in May 2011. Left panel reproduced by permission of Oxford University Press on behalf of the Royal Astronomical Society.

a random displacement from its adjacent point rather than from the mean. In such a case the variations at lower frequencies have more power. Red noise is the characteristic of several astrophysical systems including the Sun (Lu and Hamilton, 1991) and black hole binaries (Belloni and Hasinger, 1990), and it is closely related to the stochastic nature of such non-linear systems. In AGNs, over the frequency range $f = 10^{-3}$ to 10^{-5} Hz, the power spectral density of most Seyfert galaxies has a mean slope of $\alpha \sim 2.0$ in the 2 – 10 keV band, exhibiting no characteristic timescales (González-Martín and Vaughan, 2012), and indicating that red-noise steeply decreases at higher frequencies (that is shorter time scales). In some AGN there is a break in the PSD slope at $f = 2 \times 10^{-4}$ Hz, from a much flatter slope of 2 at lower frequencies to a steeper slope of 3 at higher frequencies, and the break is connected with the black hole mass. This is similar to the three slope PSD detected in black hole binaries (BHB): $\alpha \sim 0$ for low frequencies (<0.2 Hz), $\alpha \sim 1$ for intermediate frequencies (~0.2 – 3 Hz) and $\alpha \sim 2$ at higher frequencies, above 3 Hz (Vaughan et al., 2003b).

2.3.2 Quasi-periodic-oscillation (QPO)

The origin of QPOs in AGN are highly debated, they are still very rare and they have mostly been discovered in the 2 – 10 keV or harder X-ray bands. For example, such QPOs have been found at 2.6×10^{-4} Hz (~1 hour) in RE J1034 + 396 (Gierliński et al., 2008; Alston et al., 2014; 2016), at 1.5×10^{-4} Hz (~2 hours) in MS 2254.9–3712 (Alston et al., 2015), at 2.7×10^{-4} Hz (~1 hour) in 1H 0707–495 (Pan et al., 2016). A QPO of a period of ~3.8 hours was detected from an ultra-soft AGN candidate 2XMM J123103.2 + 110648 (Lin et al., 2013). A systematic study of AGN X-ray variability in a sample of 104 sources in search for QPOs detected only two sources with QPOs (González-Martín and Vaughan, 2012). Very recently a recurrent QPO has been discovered in the post-changing-look AGN 1ES 1927 + 654, where the QPO frequency increased from ~0.9 mHz to ~2.3 mHz over a period of 2 years[2] (Nature, in press).

2.3.3 X-ray flares

X-ray flares with different amplitude at different timescales are common in AGN. Typically, flares can exhibit flux increases of ~5 – 10 times over time spans ranging from hours to days (Gallo et al., 2019; Lawther et al., 2023; Wilkins et al., 2022; Reeves et al., 2021; Ding et al., 2022). During X-ray flares, a spectral softening (softer-when-brighter) and a decreasing reflection fraction have been observed in some AGNs (e.g., Mrk 335 Gallo et al., 2019, 1H 0707–495 Wilkins et al., 2014). In Mrk 335, the decade-long low flux state has been marked by occasional X-ray "flares," (see Figure 4 left panel) which have sometimes brightened by a factor of 50 within a single day (Grupe et al., 2012; Wilkins and Gallo, 2015a; Gallo et al., 2019). In some highly accreting, low SMBH mass AGN, X-ray flares

2 https://arxiv.org/abs/2501.01581

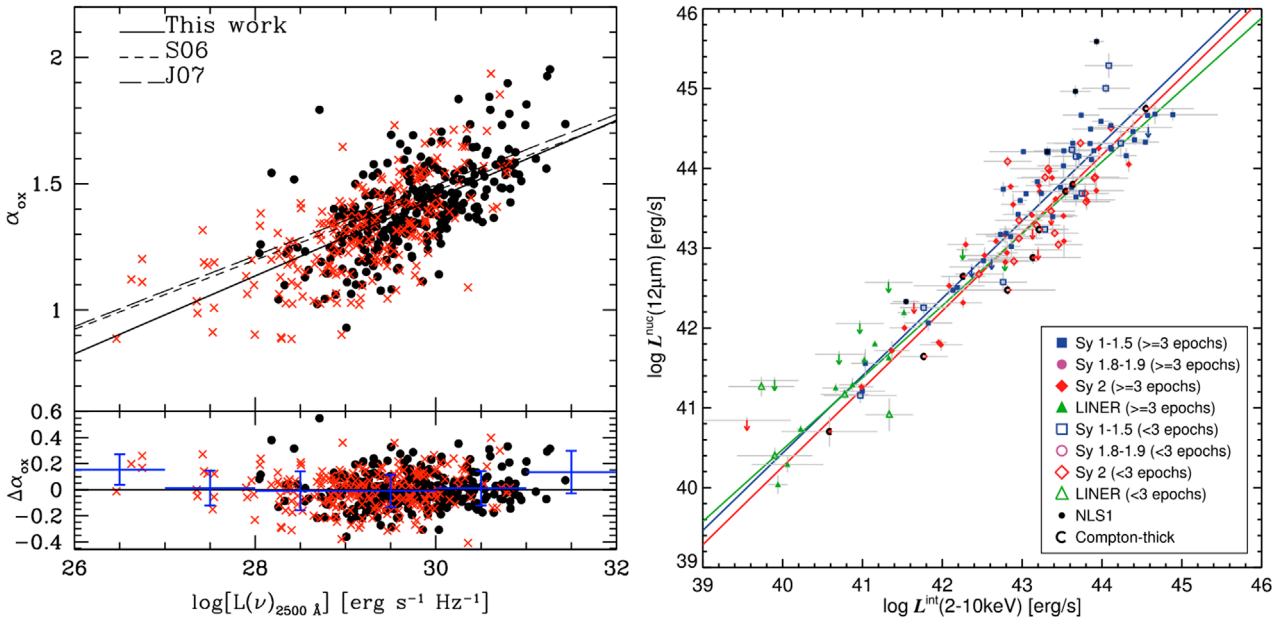

FIGURE 5
Relationship between AGN corona and its surroundings Left: The α_{OX} vs. $L_{m2500Å}$ correlation, a relation connecting the accretion disk emission (UV) and coronal emission (Lusso et al., 2010). S06 and J07 refers to Steffen et al. (2006) and Just et al. (2007) respectively. Right: The tight correlation between the spatially resolved nuclear IR emission $L_{12\mu}$ with the coronal X-ray emission (Asmus et al., 2015), indicating a close relationship between the corona and the torus. Right panel reproduced by permission of Oxford University Press on behalf of the Royal Astronomical Society. Left panel reproduced with permission © ESO.

have been linked to the radial expansion of the corona over the accretion disk: the corona appears brighter when it is more extended outward, while it dims when it is compact and located closer to the SMBH (e.g., Wilkins et al., 2014). Extreme variability and flares in AGN corona suggest that the compact corona must be a dynamic structure since the time scales for heating and cooling processes for the hot electrons are less than the light crossing time of the corona (Fabian et al., 2015), which prevents the system to settle down to an equilibrium. In addition, the plasma properties also change during a flare. For example, Wilkins et al. (2022) found that during a flare, the cutoff energy E_C of the primary energy continuum dropped from 140^{+100}_{-20} keV to 45^{+40}_{-9} keV. Another example is the Seyfert 1 galaxy I Zwicky 1 that also showed such dramatic changes in the plasma properties, when the corona rapidly cooled from E_C ~200 to ~15 keV within 5 days in January 2020, as caught by *XMM-Newton* and *NuSTAR*, (Ding et al., 2022).

X-ray flaring events in many astrophysical objects are generally associated with magnetic reconnection (e.g., Petropoulou et al., 2016; Mehlhaff et al., 2020), a fundamental plasma process where magnetic energy is converted into thermal and nonthermal particle energy (e.g., Lyubarsky, 2005; Takahashi et al., 2011). Magnetic reconnection has a short dissipation time, and short flares with durations that generally do not exceed a few times $t \sim R_G/c$ should be preferentially associated with magnetic reconnection (e.g., Petropoulou et al., 2016; Christie et al., 2018). Longer flaring episodes could be associated with magnetic flux accumulation in the corona because of accretion, changing the properties of particle acceleration and thus that of the emitted photons (e.g., Liska et al., 2020; Scepi et al., 2021; Ripperda et al., 2022).

2.4 The accretion disk - corona relation

The accretion disk and the corona are energetically and geometrically related (Haardt and Maraschi, 1993; Lusso et al., 2010; Lusso and Risaliti, 2016). A direct piece of evidence of the energy-coupling between the accretion disk and corona is the significant correlation between the quantity α_{OX} and the mono-chromatic UV flux at 2500Å (See Figure 5 left panel) (Lusso and Risaliti, 2017). The parameter $\alpha_{OX} = -0.385 \log(F_{2\,keV}/F_{2500Å})$ is the ratio between the flux densities at 2 keV ($F_{2\,keV}$) and 2500Å ($F_{2500Å}$). Together, the accretion disk and corona form a tightly coupled system.

There is also a significant correlation between α_{OX} and λ_{Edd} (Lusso et al., 2010), in which the ratio between X-ray and optical flux decreases with increasing Eddington ratio λ_{Edd}, implying increased accretion leads to weaker coronal emission. It has also been noted that at sub- and super-Eddington accretion levels, the disc-corona relations are different (Huang et al., 2020). For example, the hard X-ray slope Γ and the Eddington ratio λ_{Edd} show an anti-correlation for sources with lower accretion rate $\lambda_{Edd} < 10^{-3}$. See Figure 6 left panel (Connolly et al., 2016). On the other-hand a positive correlation is detected for higher Eddington ratio sources, which indicates a softer-when-brighter behavior common in higher accretion rate AGN (McHardy et al., 1999; Shemmer et al., 2006; Sobolewska and Papadakis, 2009). Perhaps for weakly accreting AGN ($\lambda_{Edd} < 10^{-3}$), the disc-corona system transits to an advection-dominated accretion flow (ADAF), and the X-ray emission may arise from Comptonization process in ADAF (Cao, 2009).

The reverberation mapping time lags between the optical/UV and the X-rays are an important indication of disk-corona coupling

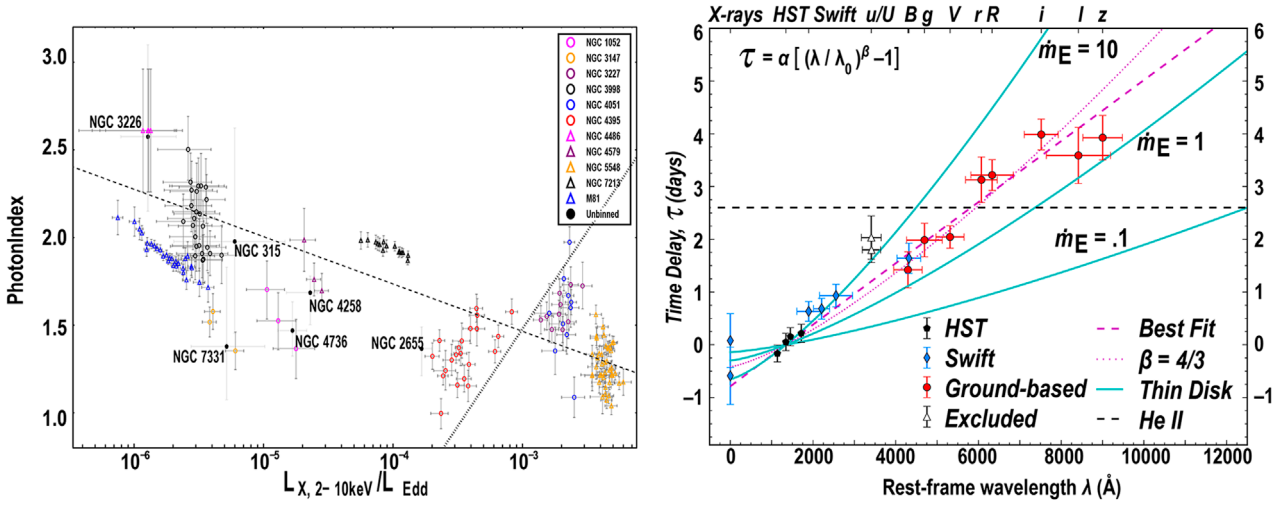

FIGURE 6
The relation between the coronal emission and AGN accretion: Left: The relation between the photon-indices Γ and $L_{2-10\ \mathrm{keV}}/L_{\mathrm{Edd}}$ (Connolly et al., 2016). At lower Eddington ratios ($\lesssim 10^{-3}$) the quantities show an anti-correlation, while for higher accretion rates the correlation is positive indicating a softer-when-brighter behavior of the corona (Cao, 2009). Right: The X-ray-optical-UV reverberation time lags measured for the source NGC 5548 (Fausnaugh et al., 2016). The trend of lag with wavelength is broadly consistent with the prediction for continuum reprocessing by a thin accretion disk with $\tau \propto \lambda^{4/3}$. Here $\dot{m}_E = L_{\mathrm{bol}}/L_{\mathrm{Edd}}$. Left panel reproduced by permission of Oxford University Press on behalf of the Royal Astronomical Society. Right panel reproduced with permission from © AAS.

TABLE 1 The empirical relations involving AGN coronal emission.

Relationship between	Equation
(1a)X-ray and UV	$\alpha_{\mathrm{OX}} = (0.154 \pm -0.010)\log L_{2500\text{Å}} - (3.176 \pm 0.223)$
(1b) X-ray and UV	$L_X \propto L_{\mathrm{UV}}^{0.7-0.8}$
(2a) Γ vs. λ_{Edd} (for $\lambda_{\mathrm{Edd}} > 0.01$)	$\Gamma = (0.41 \pm 0.09)\log\lambda_{\mathrm{Edd}} + (2.17 \pm 0.07)$
(2b) Γ vs. λ_{Edd} (for $\lambda_{\mathrm{Edd}} < 0.01$)	$\Gamma = (-0.09 \pm 0.03)\log\lambda_{\mathrm{Edd}} + (1.55 \pm 0.07)$
(3) 2 – 10 keV and Infrared	$\log \frac{L^{\mathrm{int}}_{2-10\ \mathrm{keV}}}{10^{43}\mathrm{ergs}^{-1}} = (-0.32 \pm 0.03) + (0.95 \pm 0.03)\log \frac{L^{\mathrm{nuc}}_{12\mu}}{10^{43}}\mathrm{ergs}^{-1}$
(4) $L_{2-10\ \mathrm{keV}}$ vs. OIII	$\log L_{2-10\ \mathrm{keV}} = 0.95\log L_{OIII} + 3.89$
(5) Fundamental plane of black hole	$\log L_{\mathrm{R}} = (0.60 \pm 0.11)\log L_{\mathrm{X}} + (0.78 \pm 0.11)\log M + (7.33 \pm 4.05)$
(6a) Gudel Benz relation	$L_{R,\ 5GHz} \sim 10^{-5.5} L_{2-10\ \mathrm{keV}}$
(6b) 100 GHz vs. 2–10 keV	$\log L_{100\mathrm{GHz}} = (-13.9 \pm 0.8) + (1.22 \pm 0.02)\log L_{2-10\ \mathrm{keV}}$
(7) Iwasawa-Taniguchi effect	$\log(\mathrm{EWFeK}\alpha) \propto (-0.17 \pm 0.03)\log(L_{2-10\ \mathrm{keV}})$

References: (1a): Lusso et al. (2010); Lusso and Risaliti (2016), (1b): (Just et al., 2007; Strateva et al., 2005), (2a): Risaliti et al. (2009); Kelly et al. (2008); Shemmer et al. (2008), (2b): Gu and Cao (2009), (3): (Gandhi et al., 2009; Asmus et al., 2015) (4): Saade et al. (2022); Malkan et al. (2017) (5): Merloni et al. (2003) (6a): Laor and Behar (2008) (6b): Ricci et al. (2023) (7): Iwasawa and Taniguchi (1993).
(2a) This positive correlation exists for accretion rates $\lambda_{\mathrm{Edd}} > 0.01$ (2b) For low-luminosity AGN, hence low accretion states, there exists an anti-correlation.
Note that here X-ray, $L_{\mathrm{X-ray}}$ and $L_{2-10\ \mathrm{keV}}$ has been interchangeably used and can be interpreted as similar quantity.

and serves as an important tool to understand the disk-corona geometry (see for, e.g., Peterson, 1993; Edelson et al., 2015; 2019; Cackett et al., 2021; 2023; Kara et al., 2023, and references therein). The corona is compact $\lesssim 10\,R_{\mathrm{G}}$ and centrally located relative to the accretion disk, and the UV and optical emission is expected to respond to the incident (and varying) X-ray flux, "echoing" the X-ray light curve variations after a time delay corresponding to the light-travel time across the disk (Krolik et al., 1991). For example, for the well studied case of AGN NGC 5548 (Fausnaugh et al., 2016) significant time delays between the X-rays and the optical-UV band (1158Å – 9160Å) have been detected. The trend of lag (τ) with wavelength (λ) is broadly consistent with the prediction for continuum reprocessing by a thin accretion disk with $\tau \propto \lambda^{4/3}$ (See Figure 6 right panel).

Although the correlation between the UV and X-rays are pretty well constrained in most cases, there are AGN types which show

additional complexities. The most interesting among them are changing look AGNs (CL-AGNs), which are sources that undergo a rapid change in flux and spectral state (in optical/X-rays) in a matter of months-years (see Ricci and Trakhtenbrot, 2023, for a review). Mrk 590 is a long term CL-AGN where the UV and X-rays are well correlated, but UV response to X-ray changes is lagged by ~3 days indicating a complex reprocessing geometry (a lamp-post geometry would predict a zero time lag, see for, e.g., Lawther et al., 2023). In the most enigmatic rapid CL-AGN 1ES 1927 + 654, the situation is more extreme, with no correlation between the UV and X-ray emission during the violent event (Trakhtenbrot et al., 2019; Laha et al., 2022; Ricci et al., 2021). The right panel of Figure 4 shows the absolutely uncorrelated behavior of the X-rays and UV for this source. The X-ray coronal emission of 1ES 1927 + 654 completely vanished a few months after the violent optical outburst, while the UV was still bright and dropping at a rate $\propto t^{-0.91\pm0.04}$. The corona reappeared after ~4 months at 10 times the previous luminosity (Trakhtenbrot et al., 2019; Ricci et al., 2020; 2021; Laha et al., 2022; Masterson et al., 2022), finally reaching its normal state in about ~4 years. In these extreme situations of AGN accretion, the standard disk-corona relations may not hold.

2.5 Coronae and high-energy neutrinos

Systematic searches for neutrino excess above atmospheric and cosmic backgrounds with the IceCube detector have detected 79^{+22}_{-20} neutrinos at TeV energies from the nearby AGN NGC 1068 with a significance of ~4.2σ (IceCube Collaboration et al., 2022). Notably, the isotropic neutrino luminosity ($L_\nu = 2.9^{+1.1}_{-1.1} \times 10^{42}\,\mathrm{erg\,s^{-1}}$) in the 1.5–15 TeV range exceeds both the gamma-ray luminosity ($L = 1.6 \times 10^{41}\,\mathrm{erg\,s^{-1}}$) in the 100 MeV–100 GeV range and the upper limits on gamma-ray luminosity above 200 GeV (Aartsen et al., 2020; IceCube Collaboration et al., 2022). This suggests the AGN's central engine (the X-ray corona), which is opaque to gamma-rays, significantly contributes to neutrino production (e.g., Fang et al., 2023; Murase et al., 2020; Inoue et al., 2020; Eichmann et al., 2022; Mbarek et al., 2024; Fiorillo et al., 2024; Padovani et al., 2024). Other AGNs also show hints of neutrino emission, with future deeper follow-ups expected to enhance detection significance (Neronov et al., 2023; Murase et al., 2024). Beyond AGNs, X-ray binary coronae have been proposed as potential sources of Galactic neutrinos detected by IceCube (Fang et al., 2024).

The highly magnetized black hole coronae (e.g., Beloborodov, 2017; Hooper and Plant, 2023; Grošelj et al., 2024; Nättilä, 2024; Mbarek et al., 2024) support two primary mechanisms for accelerating protons responsible for coronal neutrino production. First, magnetic reconnection in large current sheets near the black hole, with strong guide fields, can accelerate particles to extreme energies (Fiorillo et al., 2024). Second, magnetized turbulence allows particles to be initially energized by reconnection and subsequently re-accelerated within the turbulent corona (Mbarek et al., 2024). These high-energy protons interact with the corona's dense photon fields, producing the observed neutrino signal. While purely leptonic models have also been suggested (Hooper and Plant, 2023), it remains unclear how electrons could achieve the TeV-scale energies required for such scenarios.

2.6 The empirical relations involving corona

Here we list the most important empirical relations involving emission from the X-ray corona and that produced by other AGN components (see Table 1 for a list).

(1) X-ray and UV: As noted earlier, the disk and the corona emission are very tightly related, showing a strong correlation between $\alpha_{\rm OX}$ vs. $L_{2500\text{Å}}$ (Lusso et al., 2010; Bisogni et al., 2021).

(2) $\Gamma - \lambda_{\rm Edd}$: A correlation exists between Γ and $\lambda_{\rm Edd}$ ($\Gamma \sim 0.3 \times \log\lambda_{\rm Edd} + 2$) such that sources with $\lambda_{\rm Edd} > 0.3$ have a very steep slope of $\Gamma > 2$ (Shemmer et al., 2008; Risaliti et al., 2009; Brightman et al., 2013). The correlation can be explained as increased UV emission from the accretion disk due to high accretion rate can lead to radiative cooling of the X-ray corona and hence lowering of the electron temperature (that is a steeper X-ray spectrum). The left panel of Figure 6 shows this behavior between Γ vs. $L_{2-10\,\rm keV}/L_{\rm Edd}$, where we find that the higher accreting sources show a positive correlation between the two quantities, while for very low accreting sources, there is an anti-correlation (Fausnaugh et al., 2016; Gu and Cao, 2009). By simulating AGN populations with an X-ray spectral Comptonization model, Ricci et al. (2018) showed that Comptonizing plasma with temperatures and compactness lying along the pair line can straightforwardly explain the positive correlation between Γ and the Eddington ratio.

A few studies involving high $\lambda_{\rm Edd}$ sources (with $L_{\rm bol} = 10^{46}\,\mathrm{erg\,s^{-1}}$) did not detect any correlation between Γ and $\lambda_{\rm Edd}$ (Laurenti et al., 2022; Liu et al., 2021). We note here that these highly accreting sources have higher radiation pressure from the accretion disk which could affect the structure and efficiency of the accretion disc-corona system, and hence one would expect different behavior between UV and X-rays. Similar lack of $\Gamma - \lambda_{\rm Edd}$ has been found in a hard X-ray study of a sample of nearby AGN (Kamraj et al., 2022).

(3) $L_{12\mu}$ **vs.** $L_{2-10\,\rm keV}$: The spatially resolved core IR luminosity at 12μ is correlated very strongly with the $2-10$ keV X-ray emission (Gandhi et al., 2009; Asmus et al., 2015). See Figure 5 right panel.

(4) $L_{2-10\,\rm keV}$ vs. OIII: The hard X-rays are correlated with the optical emission line intensity (Bassani et al., 1999; Malkan et al., 2017; Saade et al., 2022).

(5) Fundamental plane of BH: The X-ray luminosity ($L_{2-10\,\rm keV}$), the radio luminosity ($L_{\rm 5GHz}$), and central black hole mass ($M_{\rm BH}$) in accreting systems have long been suggested to be interrelated (Tananbaum et al., 1983), and this connection has since been further established (Worrall et al., 1987; Merloni et al., 2003; Miller et al., 2011; Zhu et al., 2020). The relation between these three quantities potentially serves as an indicator of similar physics in action across different mass scales of accreting systems. However, recent studies with very high spatial resolution in radio band found that the core radio

luminosity ($L_{5\mathrm{GHz}}$) is consistently lower than that predicted by the fundamental plane relation, and the relation only holds true if we consider the extended radio emission from the host galaxy (Fischer et al., 2021).

(6) The mm and X-ray relation: As mentioned earlier, AGN show a strong correlation between their X-ray and radio luminosity at 5–200 GHz with $L_{\mathrm{R}}/L_{\mathrm{X-ray}} \sim 10^{-5.5}$ (Ricci et al., 2023; Behar et al., 2015; 2018; Kawamuro et al., 2022). As noted in the introduction, at lower radio frequencies (< 45 GHz) synchrotron self absorption prevents a direct view of the coronal radio emission.

(7) $L_{2-10\,\mathrm{keV}}$ vs. Hβ-FWHM and Hα luminosity: It has been observed that the X-ray luminosity correlates well with the broad Hβ full-width-at-half-maximum (FWHM) and the Hα luminosity. (Laor et al., 1997; Brandt et al., 1997; Shemmer et al., 2006).

(8) The Iwasawa-Taniguchi effect: Also known as the X-ray Baldwin effect, is the anti-correlation between the equivalent width of the Fe Kα emission and the 2 – 10 keV flux (Iwasawa and Taniguchi, 1993; Page et al., 2004).

3 List of open questions

Although we have discussed numerous observational discoveries regarding AGN coronal emission, several fundamental questions continue to elude us. We list some of the outstanding questions below, that, if answered, will improve our understanding of, not only the corona, but also how AGN operate.

- Since corona is found ubiquitously in AGN, is there something fundamental about the accretion process that produces it? The corona is a unique physical entity found in most accreting systems including black hole binaries (BHBs) and AGN. Studies have found similarities in coronal behavior of AGN and BHBs, lying at the two ends of black hole mass scales, suggesting that the AGN accretion-disk and corona are just a scaled-up version of those found in BHBs (McHardy et al., 2006), with the underlying physics being the same. Possibly the magnetic fields that thread the accretion disk creates and sustains the corona in these accreting systems, whose physics remains similar across a large range of black hole masses ($\sim 10 - 10^9 M_{\odot}$).
- What is the geometry of the corona? The recent X-ray polarimetric results with *IXPE* point towards a more extended geometry of the corona, situated along the accretion disk plane. However, deeper polarimetric studies of larger samples of AGN in different flux states are required to understand how the geometry varies depending on accretion and X-ray luminosity states. This can only be done with the next-generation of X-ray polarimeters, as *IXPE* is sensitivity-limited. A systematic spectral and timing studies of the AGNs in rapidly changing X-ray flux states can also reveal the geometry.
- What are the main energy pumping and dissipation mechanisms in the corona? Is the corona in thermal and radiative equilibrium? Although random magnetic reconnection events can play an important role in pumping energy into the corona (Galeev et al., 1979; Di Matteo, 1998; Merloni and Fabian, 2001; Sironi and Beloborodov, 2020; Sridhar et al., 2021), we need a deeper understanding about heating and cooling processes in such a compact region, which shows constant stochastic fluctuations, and sometimes flares. Simulations coupled with observational inputs on simultaneous radiative and thermal equilibrium can shed light on this topic in the future.
- What determines the fraction of non-thermal electrons in the X-ray emitting plasma? As mentioned in the introduction, the existence of non-thermal particles in the corona would result in a distribution of photons that extends into the MeV band. This small number of high energy particles could be highly effective in seeding pair production and can share the total available energy, thus reducing the mean energy per particle and therefore decreasing the temperature of the thermal population. Thus the non-thermal fraction of particles in the corona plays an important role in balancing the temperature of the plasma. We do not understand the origin and the exact fraction of the non-thermal electrons in coronal plasma. Future simulations on magnetic reconnection events could help us understand this.
- What are coronal flares? It is not clear to us if there are particular flux/spectral states that favor the occurrence of coronal flares (rise in flux by a factor of $\gtrsim 5$ times in a few days/months). It is also still unclear if the X-ray flares are the main energy dissipation mechanisms in the corona?

4 Future perspectives

4.1 Need for future missions

Future X-ray studies on AGN corona depends on how well we can extend our spectroscopic capabilities in the hard X-rays, preferably up to ~500 keV. Currently *NuSTAR* has a bandpass up to 79 keV and constraining cut-off energy >100 keV becomes highly uncertain and model dependent. For example, the E_C estimated for NGC 5506 using the same *NuSTAR* observation by two different models found $E_{\mathrm{C}} = 720 \pm 130$ keV (Matt et al., 2015) and 110 ± 10 keV Baloković et al. (2020).

To estimate the differences in the emissivity profiles (the illumination pattern of the accretion disk due to the reflection of X-rays from the corona, convolved with general relativistic effects), and hence the coronal shape and size, we need high quality X-ray observations, both in terms of collecting area and spectral resolution. For example, missions like *Athena* with its large collecting area (Nandra et al., 2013) and the recently launched *XRISM* with its high spectral resolution (Tashiro et al., 2020) will provide the ability to distinguish between the different coronal geometries.

The exciting field of X-ray polarimetry has just taken off with the launch of IXPE. However, a small effective-area mission such as this one needs much longer integration time to constrain the polarisation degree for even a very bright AGN (~500ks needed for MCG-5-23–16 to obtain an upper limit on polarization degree Marinucci et al. (2022b)). Future X-ray polarimeters should have very large effective area not only to constrain polarization parameters at a fraction of the exposure required by IXPE, but also carry out time dependent polarimetric analysis of AGN.

High-energy neutrinos are also expected from AGN corona, and is currently opening up a huge multi-messenger avenue for AGN-coronal studies (Kheirandish et al., 2021). In the future, deeper and more sensitive studies by IceCube and other detectors will help us in understanding the relation between neutrino emission and the physical processes in an AGN corona.

4.2 Need for simulations

Coronal heating and cooling problems are among the most significant unresolved issues in astrophysics. 'Fluid' (MHD) models, by their very nature, are unable to explore the physics of non-thermal particle acceleration within the dissipation regions, where the energy from the magnetic field is transferred to particles. The corona is expected to have a good fraction (up to 30%) of non-thermal particles (Fabian et al., 2017). In MHD simulations, the energy either stays in the system as thermal energy in the particles or is removed according to some *ad hoc* prescription. This is because, most of the non-thermal acceleration occurs in 'collisionless' plasmas, where Coulomb collisions, typically an efficient means of thermalization, are explicitly neglected. Therefore, the properties of the population of non-thermal particles responsible for the emission cannot be properly captured in fluid models.

On the other hand, particle-in-cell (PIC) simulations capture the microscopic dynamics of individual particles, rather than assuming a smooth distribution of particle energies, and thus capture accurately the non-thermal processes in dissipation regions, and the nonlinear interplay between charged particles and electromagnetic fields (e.g., Chernoglazov et al., 2023; Grošelj et al., 2024; Mbarek et al., 2024; Nättilä, 2024). Moreover, PIC simulations may include consistently evolving particles and their radiative cooling effects, in the presence of photons, pair creation and annihilation processes (Grošelj et al., 2024). These features make PIC an ideal tool to study the coronal heating problem. However, PIC simulations are usually employed to study local dissipation processes on microscopic scales—scaled down from actual astrophysical scales. Therefore, simulation setups might seem ideal and somewhat disconnected from the "global properties" of the corona. More work is still required to more robustly extrapolate the results of PIC simulations to large scales (underway efforts include, e.g., Zou et al., 2024; Sridhar et al., 2024).

Author contributions

SL: Conceptualization, Funding acquisition, Methodology, Project administration, Supervision, Validation, Writing–original draft, Writing–review and editing. CR: Validation, Writing–review and editing. JM: Conceptualization, Visualization, Writing–review and editing. EB: Conceptualization, Supervision, Validation, Writing–review and editing. LG: Supervision, Writing–review and editing. FM: Writing–review and editing. RM: Writing–review and editing. AH: Writing–review and editing.

Funding

The author(s) declare that financial support was received for the research, authorship, and/or publication of this article. We have a waiver. The material is based upon work supported by NASA under award number 80GSFC21M0002.

Acknowledgments

SL acknowledges insightful discussions with Christopher Reynolds, Mitchell Begelman, Navin Sridhar and Dev Sadaula. SL thanks NASA graphics designer Jay Friedlander for his help on the cartoon in Figure 1 and other figures. CR acknowledges support from Fondecyt Regular grant 1230345, ANID BASAL project FB210003 and the China-Chile joint research fund. EB acknowledges support by a Center of Excellence of the Israel Science Foundation (grant no. 2752/19). SL and EB acknowledge support from NSF-BSF grant numbers: NSF-2407801, BSF-2023752.

Conflict of interest

The authors declare that the research was conducted in the absence of any commercial or financial relationships that could be construed as a potential conflict of interest.

Generative AI statement

The author(s) declare that no Generative AI was used in the creation of this manuscript.

Publisher's note

References

Aartsen, M. G., Ackermann, M., Adams, J., Aguilar, J. A., Ahlers, M., Ahrens, M., et al. (2020). Time-integrated neutrino source searches with 10 years of icecube data. *Phys. Rev. Lett.* 124, 051103. doi:10.1103/PhysRevLett.124.051103

Alston, W., Fabian, A., Markevičiutė, J., Parker, M., Middleton, M., and Kara, E. (2016). Quasi periodic oscilations in active galactic nuclei. *Astron. Nachrichten* 337, 417–422. doi:10.1002/asna.201612323

Alston, W. N., Markeviciute, J., Kara, E., Fabian, A. C., and Middleton, M. (2014). Detection of a QPO in five *XMM–Newton* observations of RE J1034+396. *Detect. a QPO five Newt. observations RE J1034+396* 445, L16–L20. doi:10.1093/mnrasl/slu127

Alston, W. N., Parker, M. L., Markevičiūtė, J., Fabian, A. C., Middleton, M., Lohfink, A., et al. (2015) *Discovery of an 2-h high-frequency X-ray QPO and iron Kα reverberation in the active galaxy MS 2254*, 449, 467–476. doi:10.1093/mnras/stv351

Arnaud, K. A. (1996). *XSPEC: the first ten years. In astronomical data analysis Software and systems V*. Editors G. H. Jacoby, and J. Barnes (Astronomical Society of the Pacific Conference Series), 101.

Asmus, D., Gandhi, P., Hönig, S. F., Smette, A., and Duschl, W. J. (2015). The subarcsecond mid-infrared view of local active galactic nuclei – II. The mid-infrared–X-ray correlation. *mid-infrared-X-ray Correl.* 454, 766–803. doi:10.1093/mnras/stv1950

Balbus, S. A., and Hawley, J. F. (1998). Instability, turbulence, and enhanced transport in accretion disks. *Rev. Mod. Phys.* 70, 1–53. doi:10.1103/RevModPhys.70.1

Baldi, R. D., Laor, A., Behar, E., Horesh, A., Panessa, F., McHardy, I., et al. (2022). The PG-RQS survey. Building the radio spectral distribution of radio-quiet quasars. I. The 45-GHz data. *45-GHz data* 510, 1043–1058. doi:10.1093/mnras/stab3445

Baloković, M., Harrison, F. A., Madejski, G., Comastri, A., Ricci, C., Annuar, A., et al. (2020). NuSTAR survey of obscured swift/BAT-selected active galactic nuclei. II. Median high-energy cutoff in Seyfert II hard X-ray spectra. *Median High-energy Cutoff Seyfert II Hard X-Ray Spectra* 905, 41. doi:10.3847/1538-4357/abc342

Barthelmy, S. D., Barbier, L. M., Cummings, J. R., Fenimore, E. E., Gehrels, N., Hullinger, D., et al. (2005). The burst alert telescope (BAT) on the SWIFT midex mission. *SSRv* 120, 143–164. doi:10.1007/s11214-005-5096-3

Bassani, L., Dadina, M., Maiolino, R., Salvati, M., Risaliti, G., Della Ceca, R., et al. (1999). A three-dimensional diagnostic diagram for Seyfert 2 galaxies: probing X-ray absorption and Compton thickness. *ApJS* 121, 473–482. doi:10.1086/313202

Behar, E., Baldi, R. D., Laor, A., Horesh, A., Stevens, J., and Tzioumis, T. (2015). Discovery of millimetre-wave excess emission in radio-quiet active galactic nuclei. *Mon. Not. R. Astron. Soc., Discov. millimetre-wave excess Emiss. radio-quiet Act. galactic Nucl.* 451, 517–526. doi:10.1093/mnras/stv988

Behar, E., Vogel, S., Baldi, R. D., Smith, K. L., and Mushotzky, R. F. (2018). The mm-wave compact component of an AGN. *Mon. Not. R. Astron. Soc., mm-wave compact Compon. AGN* 478, 399–406. doi:10.1093/mnras/sty850

Beheshtipour, B., Krawczynski, H., and Malzac, J. (2017). The X-ray polarization of the accretion disk coronae of active galactic nuclei. *Astrophys. J., X-Ray Polariz. Accretion Disk Coronae Act. Galactic Nucl.* 850, 14. doi:10.3847/1538-4357/aa906a

Belloni, T., and Hasinger, G. (1990). An atlas of aperiodic variability in HMXB. *A&A* 230, 103–119.

Beloborodov, A. M. (2017). Radiative magnetic reconnection near accreting black holes. *Astrophys. J. Radiat. Magn. Reconnect. Near Accreting Black Holes* 850, 141. doi:10.3847/1538-4357/aa8f4f

Bisogni, S., Lusso, E., Civano, F., Nardini, E., Risaliti, G., Elvis, M., et al. (2021). The Chandra view of the relation between X-ray and UV emission in quasars. *A&* 655, A109. doi:10.1051/0004-6361/202140852

Brandt, W. N., Mathur, S., and Elvis, M. (1997). A comparison of the hard ASCA spectral slopes of broad- and narrow-line Seyfert 1 galaxies. *Mon. Not. R. Astron. Soc., A Comp. hard ASCA Spectr. slopes broad- narrow-line Seyfert 1 galaxies* 285, L25–L30. doi:10.1093/mnras/285.3.L25

Brenneman, L. W., Madejski, G., Fuerst, F., Matt, G., Elvis, M., Harrison, F. A., et al. (2014). Measuring the coronal properties of IC 4329A with*NuSTAR*. *Astrophys. J., Meas. Coronal Prop. IC 4329A NuSTAR* 781, 83. doi:10.1088/0004-637X/781/2/83

Brightman, M., Silverman, J. D., Mainieri, V., Ueda, Y., Schramm, M., Matsuoka, K., et al. (2013). A statistical relation between the X-ray spectral index and Eddington ratio of active galactic nuclei in deep surveys. *Mon. Not. R. Astron. Soc., A Stat. Relat. between X-ray Spectr. index Eddingt. ratio Act. galactic Nucl. deep Surv.* 433, 2485–2496. doi:10.1093/mnras/stt920

Buisson, D. J. K., Fabian, A. C., and Lohfink, A. M. (2018). Coronal temperatures of the AGN ESO 103–035 and IGR 2124.7+5058 from NuSTAR observations. *7+5058 NuSTAR observations* 481, 4419–4426. doi:10.1093/mnras/sty2609

Cackett, E. M., Bentz, M. C., and Kara, E. (2021). Reverberation mapping of active galactic nuclei: from X-ray corona to dusty torus. *iScience* 24, 102557. doi:10.1016/j.isci.2021.102557

Cackett, E. M., Gelbord, J., Barth, A. J., De Rosa, G., Edelson, R., Goad, M. R., et al. (2023). AGN STORM 2. IV. Swift X-ray and ultraviolet/optical monitoring of Mrk 817. *Astrophys. J., AGN STORM 2. IV. Swift X-Ray Ultraviolet/Optical Monit. Mrk 817* 958, 195. doi:10.3847/1538-4357/acfdac

Cackett, E. M., Zoghbi, A., Reynolds, C., Fabian, A. C., Kara, E., Uttley, P., et al. (2014). Modelling the broad Fe Kα reverberation in the AGN NGC 4151. *Mon. Not. R. Astron. Soc., Model. broad Fe Kα reverberation AGN NGC 4151* 438, 2980–2994. doi:10.1093/mnras/stt2424

Cao, X. (2009). An accretion disc-corona model for X-ray spectra of active galactic nuclei. *Mon. Not. R. Astron. Soc., An accretion disc-corona Model. X-ray spectra Act. galactic Nucl.* 394, 207–213. doi:10.1111/j.1365-2966.2008.14347.x

Chartas, G., Kochanek, C. S., Dai, X., Poindexter, S., and Garmire, G. (2009). *Astrophys. J., X-Ray Microlensing RXJ1131-1231 HE1104-1805* 693, 174–185. doi:10.1088/0004-637X/693/1/174

Chernoglazov, A., Hakobyan, H., and Philippov, A. (2023). High-energy radiation and ion acceleration in three-dimensional relativistic magnetic reconnection with strong synchrotron cooling. *Astrophys. J., High-energy Radiat. Ion Accel. Three-dimensional Relativistic Magnetic Reconnect. Strong Synchrotron Cool.* 959, 122. doi:10.3847/1538-4357/acffc6

Christie, I. M., Petropoulou, M., Sironi, L., and Giannios, D. (2018). Radiative signatures of plasmoid-dominated reconnection in blazar jets. *Mon. Notices R. Astronomical Soc.* 482, 65–82. doi:10.1093/mnras/sty2636

Connolly, S. D., McHardy, I. M., Skipper, C. J., and Emmanoulopoulos, D. (2016). Long-term X-ray spectral variability in AGN from the Palomar sample observed by Swift. *Mon. Not. R. Astron. Soc.* 459, 3963–3985. doi:10.1093/mnras/stw878

Cooke, B. A., Ricketts, M. J., Maccacaro, T., Pye, J. P., Elvis, M., Watson, M. G., et al. (1978). The Ariel V (SSI) catalogue of high galactic latitude (b° > 10) X-ray sources. *Mon. Not. R. Astron. Soc., Ariel V (SSI) catalogue high galactic latitude* 182, 489–515. doi:10.1093/mnras/182.3.489

Cowperthwaite, P. S., and Reynolds, C. S. (2014). *Astrophys. J., Nonlinear Dyn. Accretion Disks Stoch. Viscosity* 791, 126. doi:10.1088/0004-637X/791/2/126

Dai, Y., Auchère, F., Vial, J. C., Tang, Y. H., and Zong, W. G. (2010). *Astrophys. J., Large-scale Extreme-Ultraviolet Disturbances Assoc. a Limb Coronal Mass Ejection* 708, 913–919. doi:10.1088/0004-637X/708/2/913

Dauser, T., García, J., Walton, D. J., Eikmann, W., Kallman, T., McClintock, J., et al. (2016). Normalizing a relativistic model of X-ray reflection. Definition of the reflection fraction and its implementation in relxill. *A&* 590, A76. doi:10.1051/0004-6361/201628135

Dauser, T., Garcia, J., Wilms, J., Böck, M., Brenneman, L. W., Falanga, M., et al. (2013). Irradiation of an accretion disc by a jet: general properties and implications for spin measurements of black holes. *Mon. Not. R. Astron. Soc., Irradiat. accretion disc by a jet general Prop. Implic. spin Meas. black holes* 430, 1694–1708. doi:10.1093/mnras/sts710

De Marco, B., Ponti, G., Cappi, M., Dadina, M., Uttley, P., Cackett, E. M., et al. (2013). Discovery of a relation between black hole mass and soft X-ray time lags in active galactic nuclei. *Mon. Not. R. Astron. Soc., Discov. a Relat. between black hole mass soft X-ray time lags Act. galactic Nucl.* 431, 2441–2452. doi:10.1093/mnras/stt339

Di Matteo, T. (1998). Magnetic reconnection: flares and coronal heating in active galactic nuclei. *Mon. Not. R. Astron. Soc., Magnetic Reconnect. flares coronal Heat. Act. galactic Nucl.* 299, L15–l20. doi:10.1046/j.1365-8711.1998.01950.x

Ding, Y., Li, R., Ho, L. C., and Ricci, C. (2022). Accretion disk outflow during the X-ray flare of the super-eddington active nucleus of I Zwicky 1. *Astrophys. J., Accretion Disk Outflow Dur. X-Ray Flare Eddingt. Act. Nucl. I Zwicky 1* 931, 77. doi:10.3847/1538-4357/ac6955

Done, C., and Fabian, A. C. (1989). The behaviour of compact non-thermal sources with pair production. *Mon. Not. R. Astron. Soc., Behav. compact non-thermal sources pair Prod.* 240, 81–102. doi:10.1093/mnras/240.1.81

Dong, R., Greene, J. E., and Ho, L. C. (2012). X-ray properties of intermediate-mass black holes in active galaxies. *Astrophys. J. Spectr. Energy Distribution Possible Evid. Intrinsically X-Ray-weak Act. Galactic Nucl.* 761, 73. doi:10.1088/0004-637X/761/1/73

Edelson, R., Gelbord, J., Cackett, E., Peterson, B. M., Horne, K., Barth, A. J., et al. (2019). The first Swift intensive AGN accretion disk reverberation mapping survey. *Survey* 870, 123. doi:10.3847/1538-4357/aaf3b4

Edelson, R., Gelbord, J. M., Horne, K., McHardy, I. M., Peterson, B. M., Arévalo, P., et al. (2015). Space telescope and optical reverberation mapping project. *II. Swift HST Reverberation Mapp. Accretion Disk NGC* 806, 129. doi:10.1088/0004-637X/806/1/129

Eichmann, B., Oikonomou, F., Salvatore, S., Dettmar, R.-J., and Tjus, J. B. (2022). Solving the multimessenger puzzle of the agn-starburst composite galaxy ngc 1068. *Astrophysical J.* 939, 43. doi:10.3847/1538-4357/ac9588

Elvis, M., Maccacaro, T., Wilson, A. S., Ward, M. J., Penston, M. V., Fosbury, R. A. E., et al. (1978). Seyfert galaxies as X-ray sources. *Mon. Not. R. Astron. Soc. Seyfert galaxies as X-ray sources* 183, 129–157. doi:10.1093/mnras/183.2.129

Elvis, M., Wilkes, B. J., McDowell, J. C., Green, R. F., Bechtold, J., Willner, S. P., et al. (1994). Atlas of quasar energy distributions. *ApJS* 95, 1. doi:10.1086/192093

Fabian, A. C., Lohfink, A., Belmont, R., Malzac, J., and Coppi, P. (2017). Properties of AGN coronae in the NuSTAR era – II. Hybrid plasma. *Hybrid. plasma* 467, 2566–2570. doi:10.1093/mnras/stx221

Fabian, A. C., Lohfink, A., Kara, E., Parker, M. L., Vasudevan, R., and Reynolds, C. S. (2015). Properties of AGN coronae in the*NuSTAR*era. *Mon. Not. R. Astron. Soc., Prop. AGN coronae NuSTAR era* 451, 4375–4383. doi:10.1093/mnras/stv1218

Fabian, A. C., Zoghbi, A., Ross, R. R., Uttley, P., Gallo, L. C., Brandt, W. N., et al. (2009). Broad line emission from iron K- and L-shell transitions in the active galaxy 1H0707-495. *Nat* 459, 540–542. doi:10.1038/nature08007

Fang, K., Halzen, F., Heinz, S., and Gallagher, J. S. (2024). Astroparticles from X-ray binary coronae. *ApJ* 975, L35. doi:10.3847/2041-8213/ad887b

Fang, K., Lopez Rodriguez, E., Halzen, F., and Gallagher, J. S. (2023). High-energy neutrinos from the inner circumnuclear region of NGC 1068. *Astrophys. J., High-energy Neutrinos Inn. Circumnuclear Region NGC 1068* 956. doi:10.3847/1538-4357/acee70

Fausnaugh, M. M., Denney, K. D., Barth, A. J., Bentz, M. C., Bottorff, M. C., Carini, M. T., et al. (2016). Space telescope and optical reverberation mapping project. *Opt. Continuum Emiss. Broadband Time Delays NGC* 821, 56. doi:10.3847/0004-637X/821/1/56

Fiorillo, D. F. G., Petropoulou, M., Comisso, L., Peretti, E., and Sironi, L. (2024). TeV neutrinos and hard X-rays from relativistic reconnection in the corona of NGC 1068. *ApJ* 961, L14. doi:10.3847/2041-8213/ad192b

Fischer, T. C., Secrest, N. J., Johnson, M. C., Dorland, B. N., Cigan, P. J., Fernandez, L. C., et al. (2021). Fundamental reference AGN monitoring experiment (FRAMEx). I. Jumping out of the plane with the VLBA. *I. Jump. Out Plane VLBA* 906, 88. doi:10.3847/1538-4357/abca3c

Galeev, A. A., Rosner, R., and Vaiana, G. S. (1979). Structured coronae of accretion disks. *Astrophys. J., Struct. coronae accretion disks* 229, 318–326. doi:10.1086/156957

Gallo, L. (2018). "X-ray perspective of Narrow-line Seyfert 1 galaxies," in *Revisiting narrow-line Seyfert 1 galaxies and their place in the universe*, 34, 034. doi:10.22323/1.328.0034

Gallo, L. C., Gonzalez, A. G., and Miller, J. M. (2021). Eclipsing the X-ray emitting region in the active galaxy NGC 6814. *ApJ* 908, L33. doi:10.3847/2041-8213/abdcb5

Gallo, L. C., Gonzalez, A. G., Waddell, S. G. H., Ehler, H. J. S., Wilkins, D. R., Longinotti, A. L., et al. (2019). Evidence for an emerging disc wind and collimated outflow during an X-ray flare in the narrow-line Seyfert 1 galaxy Mrk 335. *Mon. Not. R. Astron. Soc., Evid. Emerg. disc wind collimated outflow Dur. X-ray flare narrow-line Seyfert 1 galaxy Mrk 335* 484, 4287–4297. doi:10.1093/mnras/stz274

Gandhi, P., Horst, H., Smette, A., Hönig, S., Comastri, A., Gilli, R., et al. (2009). Resolving the mid-infrared cores of local Seyfort. *A&* 502, 457–472. doi:10.1051/0004-6361/200811368

Gaskell, C. M. (2004). Lognormal X-ray flux variations in an extreme narrow-line Seyfert 1 galaxy. *ApJ* 612, L21–L24. doi:10.1086/424565

Ghisellini, G., Haardt, F., and Matt, G. (2004). Aborted jets and the X-ray emission of radio-quiet AGNs. *A&* 413, 535–545. doi:10.1051/0004-6361:20031562

Ghosh, R., Laha, S., Meyer, E., Roychowdhury, A., Yang, X., Acosta-Pulido, J. A., et al. (2023). A reemerging bright soft X-ray state of the changing-look active galactic nucleus 1ES 1927+654: a multiwavelength view. *A Multiwavelength View* 955, 3. doi:10.3847/1538-4357/aced92

Giacconi, R., Branduardi, G., Briel, U., Epstein, A., Fabricant, D., Feigelson, E., et al. (1979). The Einstein/HEAO 2/X-ray observatory. *Astrophys. J., Einstein (HEAO 2) X-ray Observatory* 230, 540–550. doi:10.1086/157110

Gianolli, V. E., Kim, D. E., Bianchi, S., Agís-González, B., Madejski, G., Marin, F., et al. (2023). Uncovering the geometry of the hot X-ray corona in the Seyfert galaxy NGC 4151 with IXPE. *Mon. Not. R. Astron. Soc., Uncovering geometry hot X-ray corona Seyfert galaxy NGC 4151 IXPE* 523, 4468–4476. doi:10.1093/mnras/stad1697

Gierliński, M., Middleton, M., Ward, M., and Done, C. (2008). A periodicity of ˜1hour in X-ray emission from the active galaxy RE J1034+396. *Nat* 455, 369–371. doi:10.1038/nature07277

Gilli, R., Comastri, A., and Hasinger, G. (2007). The synthesis of the cosmic X-ray background in the Chandra and XMM-Newton era. *A&* 463, 79–96. doi:10.1051/0004-6361:20066334

Gleissner, T., Wilms, J., Pottschmidt, K., Uttley, P., Nowak, M. A., and Staubert, R. (2004). Long term variability of Cyg X-1. II. The rms-flux relation. *A&* 414, 1091–1104. doi:10.1051/0004-6361:20031684

Gonzalez, A. G., Wilkins, D. R., and Gallo, L. C. (2017). Probing the geometry and motion of AGN coronae through accretion disc emissivity profiles. *Mon. Not. R. Astron. Soc., Probing geometry motion AGN coronae through accretion disc emissivity profiles* 472, 1932–1945. doi:10.1093/mnras/stx2080

González-Martín, O., and Vaughan, S. (2012). X-ray variability of 104 active galactic nuclei: *XMM-Newton*power-spectrum density profiles⋆. *A&* 544, A80. doi:10.1051/0004-6361/201219008

Grandi, P., Tagliaferri, G., Giommi, P., Barr, P., and Palumbo, G. G. C. (1992). X-ray luminosity and spectral variability of hard X-ray–selected active galactic nuclei. *ApJS* 82, 93. doi:10.1086/191710

Grošelj, D., Hakobyan, H., Beloborodov, A. M., Sironi, L., and Philippov, A. (2024). Radiative particle-in-cell simulations of turbulent comptonization in magnetized black-hole coronae. *Phys. Rev. Lett., Radiat. Particle-in-Cell Simulations Turbul. Compt. Magnetized Black-Hole Coronae* 132, 085202. doi:10.1103/PhysRevLett.132.085202

Grupe, D., Komossa, S., Gallo, L. C., Longinotti, A. L., Fabian, A. C., Pradhan, A. K., et al. (2012). A remarkable long-term light curve and deep, low-state spectroscopy: Swift and XMM-Newton monitoring of the NLS1 galaxy mkn 335. *ApJS* 199. *Astrophys. J. Suppl. Ser.* 199, 28. doi:10.1088/0067-0049/199/2/28

Gu, M., and Cao, X. (2009). The anticorrelation between the hard X-ray photon index and the Eddington ratio in low-luminosity active galactic nuclei. *Mon. Not. R. Astron. Soc., anticorrelation between hard X-ray Phot. index Eddingt. ratio low-luminosity Act. galactic Nucl.* 399, 349–356. doi:10.1111/j.1365-2966.2009.15277.x

Guedel, M., and Benz, A. O. (1993). X-Ray/Microwave relation of different types of active stars. *ApJ* 405, L63. doi:10.1086/186766

Haardt, F., and Maraschi, L. (1991). A two-phase model for the X-ray emission from Seyfert galaxies. *ApJ* 380, L51. doi:10.1086/186171

Haardt, F., and Maraschi, L. (1993). X-ray spectra from two-phase accretion disks. *Astrophys. J., X-Ray Spectra Two-Phase Accretion Disks* 413, 507. doi:10.1086/173020

Harrison, F. A., Craig, W. W., Christensen, F. E., Hailey, C. J., Zhang, W. W., Boggs, S. E., et al. (2013). The*nuclear spectroscopic telescope array*(*NuSTAR*) high-energy x-ray mission. *Astrophys. J., Nucl. Spectrosc. Telesc. Array (NuSTAR) High-energy X-Ray Mission* 770, 103. doi:10.1088/0004-637X/770/2/103

Heil, L. M., Vaughan, S., and Uttley, P. (2012). The ubiquity of the rms-flux relation in black hole X-ray binaries. *Mon. Not. R. Astron. Soc.* 422, 2620–2631. doi:10.1111/j.1365-2966.2012.20824.x

Hooper, D., and Plant, K. (2023). Leptonic model for neutrino emission from active galactic nuclei. *Phys. Rev. Lett., Lept. Model. Neutrino Emiss. Act. Galactic Nucl.* 131, 231001. doi:10.1103/PhysRevLett.131.231001

Huang, J., Luo, B., Du, P., Hu, C., Wang, J.-M., and Li, Y.-J. (2020). On the relation between the hard X-ray photon index and accretion rate for super-eddington accreting quasars. *Astrophys. J., Relat. between Hard X-Ray Phot. Index Accretion Rate Eddingt. Accreting Quasars* 895, 114. doi:10.3847/1538-4357/ab9019

IceCube Collaboration, Abbasi, R., Ackermann, M., Adams, J., Aguilar, J. A., Ahlers, M., et al. (2022). Evidence for neutrino emission from the nearby active galaxy NGC 1068. *Science* 378, 538–543. doi:10.1126/science.abg3395

Ingram, A., Ewing, M., Marinucci, A., Tagliacozzo, D., Rosario, D. J., Veledina, A., et al. (2023). The X-ray polarization of the Seyfert 1 galaxy IC 4329A. *Mon. Not. R. Astron. Soc., X-ray Polariz. Seyfert 1 galaxy IC 4329A* 525, 5437–5449. doi:10.1093/mnras/stad2625

Ingram, A., and van der Klis, M. (2013). An exact analytic treatment of propagating mass accretion rate fluctuations in X-ray binaries. *Mon. Not. R. Astron. Soc., An exact Anal. Treat. propagating mass accretion rate fluctuations X-ray Bin.* 434, 1476–1485. doi:10.1093/mnras/stt1107

Inoue, Y., Khangulyan, D., and Doi, A. (2020). On the origin of high-energy neutrinos from NGC 1068: the role of nonthermal coronal activity. *ApJ* 891, L33. doi:10.3847/2041-8213/ab7661

Iwasawa, K., and Taniguchi, Y. (1993). The X-ray Baldwin effect. *ApJ* 413, L15. doi:10.1086/186948

Just, D. W., Brandt, W. N., Shemmer, O., Steffen, A. T., Schneider, D. P., Chartas, G., et al. (2007). The X-ray properties of the most luminous quasars from the sloan digital sky survey. *Survey* 665, 1004–1022. doi:10.1086/519990

Kamraj, N., Brightman, M., Harrison, F. A., Stern, D., García, J. A., Baloković, M., et al. (2022). X-ray coronal properties of swift/BAT-selected Seyfert 1 active galactic nuclei. *Astrophys. J., X-Ray Coronal Prop. Swift/BAT-selected Seyfert 1 Act. Galactic Nucl.* 927, 42. doi:10.3847/1538-4357/ac45f6

Kara, E., Alston, W. N., Fabian, A. C., Cackett, E. M., Uttley, P., Reynolds, C. S., et al. (2016). A global look at X-ray time lags in Seyfert galaxies. *Mon. Not. R. Astron. Soc., A Glob. look A. T. X-ray time lags Seyfert galaxies* 462, 511–531. doi:10.1093/mnras/stw1695

Kara, E., Barth, A. J., Cackett, E. M., Gelbord, J., Montano, J., Li, Y.-R., et al. (2023). UV–Optical disk reverberation lags despite a faint X-ray corona in the active galactic Nucleus Mrk 335. *Astrophys. J., UV-Optical Disk Reverberation Lags despite a Faint X-Ray Corona Act. Galactic Nucl. Mrk 335* 947, 62. doi:10.3847/1538-4357/acbcd3

Kara, E., Fabian, A. C., Cackett, E. M., Miniutti, G., and Uttley, P. (2013). Revealing the X-ray source in IRAS 13224–3809 through flux-dependent reverberation lags. *Mon. Not. R. Astron. Soc., Reveal. X-ray source IRAS 13224-3809 through flux-dependent reverberation lags* 430, 1408–1413. doi:10.1093/mnras/stt024

Kara, E., García, J. A., Lohfink, A., Fabian, A. C., Reynolds, C. S., Tombesi, F., et al. (2017). The high-Eddington NLS1 Ark 564 has the coolest corona. *Mon. Not. R. Astron. Soc., Eddingt. NLS1 Ark 564 has Cool. corona* 468, 3489–3498. doi:10.1093/mnras/stx792

Kawamuro, T., Ricci, C., Imanishi, M., Mushotzky, R. F., Izumi, T., Ricci, F., et al. (2022). BASS XXXII: studying the nuclear mm-wave continuum emission of AGNs with ALMA at scales 100-200 pc. *arXiv e-prints , arXiv:2208*, 03880. doi:10.3847/1538-4357/ac8794

Kelly, B. C., Bechtold, J., Trump, J. R., Vestergaard, M., and Siemiginowska, A. (2008). Observational constraints on the dependence of radio-quiet quasar X-ray emission on black hole mass and accretion rate. *ApJS* 176, 355–373. doi:10.1086/533440

Kelly, B. C., Sobolewska, M., and Siemiginowska, A. (2011). *Astrophys. J., A Stoch. Model. Luminosity Fluctuations Accreting Black Holes* 730, 52. doi:10.1088/0004-637X/730/1/52

Kheirandish, A., Murase, K., and Kimura, S. S. (2021). High-energy neutrinos from magnetized coronae of active galactic nuclei and prospects for identification of

Seyfert galaxies and quasars in neutrino telescopes. *Astrophys. J., High-energy Neutrinos Magnetized Coronae Act. Galactic Nucl. Prospects Identif. Seyfert Galaxies Quasars Neutrino Telesc.* 922, 45. doi:10.3847/1538-4357/ac1c77

King, A. R., Pringle, J. E., West, R. G., and Livio, M. (2004). Variability in black hole accretion discs. *Mon. Not. R. Astron. Soc., Var. black hole accretion discs* 348, 111–122. doi:10.1111/j.1365-2966.2004.07322.x

Kotov, O., Churazov, E., and Gilfanov, M. (2001). On the X-ray time-lags in the black hole candidates. *Mon. Not. R. Astron. Soc., X-ray time-lags black hole candidates* 327, 799–807. doi:10.1046/j.1365-8711.2001.04769.x

Krawczynski, H., Muleri, F., Dovčiak, M., Veledina, A., Rodriguez Cavero, N., Svoboda, J., et al. (2022). Polarized x-rays constrain the disk-jet geometry in the black hole x-ray binary Cygnus X-1. *Science* 378, 650–654. doi:10.1126/science.add5399

Krolik, J. H., Horne, K., Kallman, T. R., Malkan, M. A., Edelson, R. A., and Kriss, G. A. (1991). Ultraviolet variability of NGC 5548 - dynamics of the continuum production region and geometry of the broad-line region. *Astrophys. J., Ultrav. Var. NGC 5548 Dyn. Continuum Prod. Region Geometry Broad-Line Region* 371, 541. doi:10.1086/169918

Laha, S., Meyer, E., Roychowdhury, A., Becerra Gonzalez, J., Acosta-Pulido, J. A., Thapa, A., et al. (2022). A radio, optical, UV, and X-ray view of the enigmatic changing-look active galactic nucleus 1ES 1927+654 from its pre-to postflare states. *Astrophys. J., A Radio, Opt. UV, X-Ray View Enigmatic Changing-look Act. Galactic Nucl. 1ES 1927+654 Its Pre- Postflare States* 931, 5. doi:10.3847/1538-4357/ac63aa

Laor, A., and Behar, E. (2008). On the origin of radio emission in radio-quiet quasars. *Mon. Not. R. Astron. Soc., Orig. radio Emiss. radio-quiet quasars* 390, 847–862. doi:10.1111/j.1365-2966.2008.13806.x

Laor, A., Fiore, F., Elvis, M., Wilkes, B. J., and McDowell, J. C. (1997). The soft X-ray properties of a complete sample of optically selected quasars. II. Final results. *Final Results* 477, 93–113. doi:10.1086/303696

Laurenti, M., Piconcelli, E., Zappacosta, L., Tombesi, F., Vignali, C., Bianchi, S., et al. (2022). X-ray spectroscopic survey of highly accreting AGN. *A&* 657, A57. doi:10.1051/0004-6361/202141829

Lawrence, A., Watson, M. G., Pounds, K. A., and Elvis, M. (1987). Low-frequency divergent X-ray variability in the Seyfert galaxy NGC4051. *Nat* 325, 694–696. doi:10.1038/325694a0

Lawther, D., Vestergaard, M., Raimundo, S., Koay, J. Y., Peterson, B. M., Fan, X., et al. (2023). Flares in the changing look AGN Mrk 590 - I. The UV response to X-ray outbursts suggests a more complex reprocessing geometry than a standard disc. *Mon. Not. R. Astron. Soc.* 519, 3903–3922. doi:10.1093/mnras/stac3515

Lin, D., Irwin, J. A., Godet, O., Webb, N. A., and Barret, D. (2013). A ˜3.8 hr periodicity from an ultrasoft active galactic nucleus candidate. *ApJ* 776, L10. doi:10.1088/2041-8205/776/1/L10

Liska, M., Tchekhovskoy, A., and Quataert, E. (2020). Large-scale poloidal magnetic field dynamo leads to powerful jets in GRMHD simulations of black hole accretion with toroidal field. *Mon. Not. R. Astron. Soc., Large-scale poloidal magnetic field dynamo leads powerful jets GRMHD simulations black hole accretion toroidal field* 494, 3656–3662. doi:10.1093/mnras/staa955

Liu, H., Luo, B., Brandt, W. N., Brotherton, M. S., Gallagher, S. C., Ni, Q., et al. (2021). On the observational difference between the accretion disk–corona connections among super- and sub-eddington accreting active galactic nuclei. *Astrophys. J., Observational Differ. between Accretion Disk-Corona Connect. among Super- Eddingt. Accreting Act. Galactic Nucl.* 910, 103. doi:10.3847/1538-4357/abe37f

Lu, E. T., and Hamilton, R. J. (1991). Avalanches and the distribution of solar flares. *ApJ* 380, L89. doi:10.1086/186180

Lumb, D. H., Schartel, N., and Jansen, F. A. (2012). X-Ray multi-mirror mission (XMM-Newton) observatory. *Opt. Eng.* 51, 011009–011011. doi:10.1117/1.OE.51.1.011009

Lusso, E., Comastri, A., Vignali, C., Zamorani, G., Brusa, M., Gilli, R., et al. (2010). The X-ray to optical-UV luminosity ratio of X-ray selected type 1 AGN in XMM-COSMOS. *A&* 512, A34. doi:10.1051/0004-6361/200913298

Lusso, E., and Risaliti, G. (2016). *Astrophys. J., Tight Relat. between X-Ray Ultrav. Luminosity Quasars* 819, 154. doi:10.3847/0004-637X/819/2/154

Lusso, E., and Risaliti, G. (2017). Quasars as standard candles. I. The physical relation between disc and coronal emission. *A&* 602, A79. doi:10.1051/0004-6361/201630079

Lyubarskii, Y. E. (1997). Flicker noise in accretion discs. *Mon. Not. R. Astron. Soc., Flicker noise accretion discs* 292, 679–685. doi:10.1093/mnras/292.3.679

Lyubarsky, Y. E. (2005). On the relativistic magnetic reconnection. *Mon. Notices R. Astronomical Soc.* 358, 113–119. doi:10.1111/j.1365-2966.2005.08767.x

Makino, F., and ASTRO-C Team (1987). *The X-ray astronomy satellite ASTRO-C*, 25, 223.

Malkan, M. A., Jensen, L. D., Rodriguez, D. R., Spinoglio, L., and Rush, B. (2017). Emission line properties of Seyfert galaxies in the 12 μm sample. *Astrophys. J., Emiss. Line Prop. Seyfert Galaxies 12 μm Sample* 846, 102. doi:10.3847/1538-4357/aa8302

Marconi, A., Risaliti, G., Gilli, R., Hunt, L. K., Maiolino, R., and Salvati, M. (2004). Local supermassive black holes, relics of active galactic nuclei and the X-ray background. *Mon. Not. R. Astron. Soc., Local supermassive black holes, relics Act. galactic Nucl. X-ray Backgr.* 351, 169–185. doi:10.1111/j.1365-2966.2004.07765.x

Marinucci, A., Muleri, F., Dovciak, M., Bianchi, S., Marin, F., Matt, G., et al. (2022a). Polarization constraints on the X-ray corona in Seyfert galaxies: MCG-05-23-16. *Galaxies MCG-05-23-16* 516, 5907–5913. doi:10.1093/mnras/stac2634

Marinucci, A., Muleri, F., Dovčiak, M., Bianchi, S., Marin, F., Matt, G., et al. (2022b). Polarization constraints on the X-ray corona in Seyfert galaxies: MCG-05-23-16. *arXiv e-prints*.

Martí-Vidal, I., Muller, S., Vlemmings, W., Horellou, C., and Aalto, S. (2015). A strong magnetic field in the jet base of a supermassive black hole. *Science* 348, 311–314. doi:10.1126/science.aaa1784

Martocchia, S., Piconcelli, E., Zappacosta, L., Duras, F., Vietri, G., Vignali, C., et al. (2017). The WISSH quasars project. III. X-ray properties of hyper-luminous quasars. *A&* 608, A51. doi:10.1051/0004-6361/201731314

Masterson, M., Kara, E., Ricci, C., García, J. A., Fabian, A. C., Pinto, C., et al. (2022). Evolution of a relativistic outflow and X-ray corona in the extreme changing-look AGN 1ES 1927+654. *Astrophys. J., Evol. a Relativistic Outflow X-Ray Corona Extreme Changing-look AGN 1ES 1927+654* 934, 35. doi:10.3847/1538-4357/ac76c0

Matt, G., Baloković, M., Marinucci, A., Ballantyne, D. R., Boggs, S. E., Christensen, F. E., et al. (2015). The hard X-ray spectrum of NGC 5506 as seen by NuSTAR. *Mon. Not. R. Astron. Soc., hard X-ray Spectr. NGC 5506 as seen by NuSTAR* 447, 3029–3033. doi:10.1093/mnras/stu2653

Mbarek, R., Philippov, A., Chernoglazov, A., Levinson, A., and Mushotzky, R. (2024). Interplay between accelerated protons, x rays and neutrinos in the corona of NGC 1068: constraints from kinetic plasma simulations. *Phys. Rev. D, Interplay between Accel. Prot. x rays neutrinos corona NGC 1068 Constraints Kinet. plasma simulations* 109. doi:10.1103/PhysRevD.109.L101306

McHardy, I., and Czerny, B. (1987). Fractal X-ray time variability and spectral invariance of the Seyfert galaxy NGC5506. *Nat* 325, 696–698. doi:10.1038/325696a0

McHardy, I. M., Gunn, K. F., Uttley, P., and Goad, M. R. (2005). MCG-6-30-15: long time-scale X-ray variability, black hole mass and active galactic nuclei high states. *Mon. Not. R. Astron. Soc.* 359, 1469–1480. doi:10.1111/j.1365-2966.2005.08992.x

McHardy, I. M., Koerding, E., Knigge, C., Uttley, P., and Fender, R. P. (2006). Active galactic nuclei as scaled-up Galactic black holes. *Nat* 444, 730–732. doi:10.1038/nature05389

McHardy, I. M., Papadakis, I. E., and Uttley, P. (1999). Temporal and spectral variability of AGN with RXTE. *Nucl. Phys. B Proc. Suppl.* 69, 509–514. doi:10.1016/S0920-5632(98)00272-2

McHardy, I. M., Papadakis, I. E., Uttley, P., Page, M. J., and Mason, K. O. (2004). Combined long and short time-scale X-ray variability of NGC 4051 with*RXTE*and*XMM-Newton*. *Mon. Not. R. Astron. Soc., Comb. long short time-scale X-ray Var. NGC 4051 RXTE Newt.* 348, 783–801. doi:10.1111/j.1365-2966.2004.07376.x

Mehlhaff, J. M., Werner, G. R., Uzdensky, D. A., and Begelman, M. C. (2020). Kinetic beaming in radiative relativistic magnetic reconnection: a mechanism for rapid gamma-ray flares in jets. *Mon. Not. R. Astron. Soc.* 498, 799–820. doi:10.1093/mnras/staa2346

Merloni, A., and Fabian, A. C. (2001). Accretion disc coronae as magnetic reservoirs. *Mon. Not. R. Astron. Soc. Accretion disc coronae as Magn. Reserv.* 321, 549–552. doi:10.1046/j.1365-8711.2001.04060.x

Merloni, A., Heinz, S., and di Matteo, T. (2003). A Fundamental Plane of black hole activity. *Mon. Not. R. Astron. Soc., A Fundam. Plane black hole activity* 345, 1057–1076. doi:10.1046/j.1365-2966.2003.07017.x

Middei, R., Marinucci, A., Braito, V., Bianchi, S., De Marco, B., Luminari, A., et al. (2022). The lively accretion disc in NGC 2992 – II. The 2019/2021 X-ray monitoring campaigns. *Mon. Not. R. Astron. Soc.* 514, 2974–2993. doi:10.1093/mnras/stac1381

Miller, B. P., Brandt, W. N., Schneider, D. P., Gibson, R. R., Steffen, A. T., and Wu, J. (2011). *Astrophys. J., X-ray Emiss. Opt. Sel. Radio-intermediate Radio-loud Quasars* 726, 20. doi:10.1088/0004-637X/726/1/20

Miller, K. A., and Stone, J. M. (2000). The Formation and structure of a strongly magnetized corona above a weakly magnetized accretion disk. *Astrophys. J., Form. Struct. a Strongly Magnetized Corona above a Weakly Magnetized Accretion Disk* 534, 398–419. doi:10.1086/308736

Miniutti, G., and Fabian, A. C. (2004). A light bending model for the X-ray temporal and spectral properties of accreting black holes. *Mon. Not. R. Astron. Soc., A light bending Model. X-ray temporal Spectr. Prop. accreting black holes* 349, 1435–1448. doi:10.1111/j.1365-2966.2004.07611.x

Mitsuda, K., Bautz, M., Inoue, H., Kelley, R. L., Koyama, K., Kunieda, H., et al. (2007). The X-ray observatory Suzaku. *PASJ* 59, S1–S7. doi:10.1093/pasj/59.sp1.S1

Morgan, C. W., Kochanek, C. S., Dai, X., Morgan, N. D., and Falco, E. E. (2008). X-Ray and optical microlensing in the lensed quasar PG 1115+080. *Astrophys. J., X-Ray Opt. Microlensing Lensed Quasar PG 1115+080* 689, 755–761. doi:10.1086/592767

Murase, K., Karwin, C. M., Kimura, S. S., Ajello, M., and Buson, S. (2024). Sub-GeV gamma rays from nearby Seyfert galaxies and implications for coronal neutrino emission. *ApJ* 961, L34. doi:10.3847/2041-8213/ad19c5

Murase, K., Kimura, S. S., and Mészáros, P. (2020). Hidden cores of active galactic nuclei as the origin of medium-energy neutrinos: critical tests with the MeV gamma-ray connection. *Phys. Rev. Lett., Hidden Cores Act. Galactic Nucl.*

as Orig. Medium-Energy Neutrinos Crit. Tests MeV Gamma-Ray Connect. 125. doi:10.1103/PhysRevLett.125.011101

Mushotzky, R. F. (1984). X-ray spectra and time variability of active galactic nuclei. *Adv. Space Res.* 3, 157–165. doi:10.1016/0273-1177(84)90081-4

Mushotzky, R. F., Done, C., and Pounds, K. A. (1993). X-ray spectra and time variability of active galactic nuclei. *ARAA* 31, 717–761. doi:10.1146/annurev.aa.31.090193.003441

Mushotzky, R. F., Marshall, F. E., Boldt, E. A., Holt, S. S., and Serlemitsos, P. J. (1980). HEAO 1 spectra of X-ray emitting Seyfert 1 galaxies. *Astrophys. J., HEAO 1 spectra X-ray Emit. Seyfert 1 galaxies* 235, 377–385. doi:10.1086/157641

Nandra, K., Barret, D., Barcons, X., Fabian, A., den Herder, J.-W., Piro, L., et al. (2013). The hot and energetic universe: a white paper presenting the science theme motivating the Athena+ mission.

Nättilä, J. (2024). Radiative plasma simulations of black hole accretion flow coronae in the hard and soft states. *Nat. Commun.* 15, 7026. doi:10.1038/s41467-024-51257-1

Neronov, A., Savchenko, D., and Semikoz, D. V. (2023). Neutrino signal from Seyfert galaxies. *arXiv e-prints*, 09018doi. arXiv:2306. doi:10.48550/arXiv.2306.09018

O'Sullivan, S. P., and Gabuzda, D. C. (2009). Magnetic field strength and spectral distribution of six parsec-scale active galactic nuclei jets. *Mon. Not. R. Astron. Soc., Magnetic field strength Spectr. distribution six parsec-scale Act. galactic Nucl. jets* 400, 26–42. doi:10.1111/j.1365-2966.2009.15428.x

Padovani, P., Resconi, E., Ajello, M., Bellenghi, C., Bianchi, S., Blasi, P., et al. (2024). Supermassive black holes and very high-energy neutrinos: the case of NGC 1068. *arXiv e-prints*. arXiv:2405.20146doi. doi:10.48550/arXiv.2405.20146

Page, K. L., O'Brien, P. T., Reeves, J. N., and Turner, M. J. L. (2004). An X-ray Baldwin effect for the narrow Fe Kα lines observed in active galactic nuclei. *Mon. Not. R. Astron. Soc.* 347, 316–322. doi:10.1111/j.1365-2966.2004.07203.x

Pan, H.-W., Yuan, W., Yao, S., Zhou, X.-L., Liu, B., Zhou, H., et al. (2016). Detection of a possible X-ray quasi-periodic oscillation in the active galactic nucleus 1H 0707-495. *ApJ* 819, L19. doi:10.3847/2041-8205/819/2/L19

Panessa, F., Baldi, R. D., Laor, A., Padovani, P., Behar, E., and McHardy, I. (2019). The origin of radio emission from radio-quiet active galactic nuclei. *Nat. Astron.* 3, 387–396. doi:10.1038/s41550-019-0765-4

Papadakis, I. E. (2004). The scaling of the X-ray variability with black hole mass in active galactic nuclei. *Mon. Not. R. Astron. Soc.* 348, 207–213. doi:10.1111/j.1365-2966.2004.07351.x

Parker, M. L., Wilkins, D. R., Fabian, A. C., Grupe, D., Dauser, T., Matt, G., et al. (2014). *Mon. Not. R. Astron. Soc., NuSTAR Spectr. Mrk 335 extreme relativistic Eff. within two gravitational radii event horizon?* 443, 1723–1732. doi:10.1093/mnras/stu1246

Peterson, B. M. (1993). Reverberation mapping of active galactic nuclei. *Publ. Astron. Soc. Pac., Reverberation Mapp. Act. Galactic Nucl.* 105, 247. doi:10.1086/133140

Petropoulou, M., Giannios, D., and Sironi, L. (2016). Blazar flares powered by plasmoids in relativistic reconnection. *Mon. Not. R. Astron. Soc., Blazar flares powered by plasmoids relativistic Reconnect.* 462, 3325–3343. doi:10.1093/mnras/stw1832

Petrucci, P. O., Haardt, F., Maraschi, L., Grandi, P., Malzac, J., Matt, G., et al. (2001). Testing comptonization models Using*BeppoSAX*Observations of Seyfert 1 galaxies. *Astrophys. J., Test. Compt. Models Using BeppoSAX Observations Seyfert 1 Galaxies* 556, 716–726. doi:10.1086/321629

Petrucci, P. O., Haardt, F., Maraschi, L., Grandi, P., Matt, G., Nicastro, F., et al. (2000). Testing comptonizing coronae on a Long*BEPPOSAX*Observation of the Seyfert 1 galaxy NGC 5548. *Astrophys. J., Test. Compt. Coronae a Long BeppoSAX Observation Seyfert 1 Galaxy NGC 5548* 540, 131–142. doi:10.1086/309319

Petrucci, P. O., Paltani, S., Malzac, J., Kaastra, J. S., Cappi, M., Ponti, G., et al. (2013). Multiwavelength campaign on Mrk 509. XII. Broad band spectral analysis. *A&* 549, A73. doi:10.1051/0004-6361/201219956

Piconcelli, E., Jimenez-Bailón, E., Guainazzi, M., Schartel, N., Rodríguez-Pascual, P. M., and Santos-Lleó, M. (2005). The XMM-Newton view of PG quasars. I. X-ray continuum and absorption. *A&* 432, 15–30. doi:10.1051/0004-6361:20041621

Reeves, J. N., Braito, V., Porquet, D., Lobban, A. P., Matzeu, G. A., and Nardini, E. (2021). The flaring X-ray corona in the quasar PDS 456. *Mon. Not. R. Astron. Soc., flaring X-ray corona quasar PDS 456* 500, 1974–1991. doi:10.1093/mnras/staa3377

Ricci, C., Chang, C.-S., Kawamuro, T., Privon, G. C., Mushotzky, R., Trakhtenbrot, B., et al. (2023). A tight correlation between millimeter and X-ray emission in accreting massive black holes from <100 mas resolution ALMA observations. *ApJ* 952, L28. doi:10.3847/2041-8213/acda27

Ricci, C., Ho, L. C., Fabian, A. C., Trakhtenbrot, B., Koss, M. J., Ueda, Y., et al. (2018). BAT AGN Spectroscopic Survey – XII. The relation between coronal properties of active galactic nuclei and the Eddington ratio. *Relat. between coronal Prop. Act. galactic Nucl. Eddingt. ratio* 480, 1819–1830. doi:10.1093/mnras/sty1879

Ricci, C., Kara, E., Loewenstein, M., Trakhtenbrot, B., Arcavi, I., Remillard, R., et al. (2020). The destruction and recreation of the X-ray corona in a changing-look active galactic nucleus. *ApJ* 898, L1. doi:10.3847/2041-8213/ab91a1

Ricci, C., Loewenstein, M., Kara, E., Remillard, R., Trakhtenbrot, B., Arcavi, I., et al. (2021). The 450 Day X-ray monitoring of the changing-look AGN 1ES 1927+654. *ApJS* 255, 7. doi:10.3847/1538-4365/abe94b

Ricci, C., and Trakhtenbrot, B. (2022). *Changing-look active galactic nuclei*. doi:10.48550/arXiv.2211.05132

Ricci, C., and Trakhtenbrot, B. (2023). Changing-look active galactic nuclei. *Nat. Astron.* 7, 1282–1294. doi:10.1038/s41550-023-02108-4

Ricci, C., Trakhtenbrot, B., Koss, M. J., Ueda, Y., Del Vecchio, I., Treister, E., et al. (2017). BAT AGN spectroscopic survey. V. X-ray properties of the Swift/BAT 70-month AGN catalog. *ApJS* 233, 17. doi:10.3847/1538-4365/aa96ad

Ripperda, B., Liska, M., Chatterjee, K., Musoke, G., Philippov, A. A., Markoff, S. B., et al. (2022). Black hole flares: ejection of accreted magnetic flux through 3D plasmoid-mediated reconnection. *ApJ* 924, L32. doi:10.3847/2041-8213/ac46a1

Risaliti, G., Elvis, M., Fabbiano, G., Baldi, A., Zezas, A., and Salvati, M. (2007). Occultation measurement of the size of the X-ray-emitting region in the active galactic nucleus of NGC 1365. *ApJ* 659, L111–L114. doi:10.1086/517884

Risaliti, G., Nardini, E., Salvati, M., Elvis, M., Fabbiano, G., Maiolino, R., et al. (2011). X-ray absorption by broad-line region clouds in Mrk 766: X-ray absorption by BLR clouds in Mrk 766. *Mon. Not. R. Astron. Soc., X-ray Absorpt. by broad-line region clouds Mrk 766* 410, 1027–1035. doi:10.1111/j.1365-2966.2010.17503.x

Risaliti, G., Young, M., and Elvis, M. (2009). The sloan digital sky survey/XMM-Newton quasar survey: correlation between X-ray spectral slope and Eddington ratio. *ApJ* 700, L6–L10. doi:10.1088/0004-637X/700/1/L6

Rothschild, R., Boldt, E., Holt, S., Serlemitsos, P., Garmire, G., Agrawal, P., et al. (1979). The cosmic X-ray experiment aboard HEAO-1. *Space Sci. Instrum.* 4, 269–301.

Rothschild, R. E., Mushotzky, F. R., Baity, W. A., Gruber, D. E., Matteson, J. L., and Peterson, L. E. (1983). 2-165 keV observations of active galaxies and the diffuse background. *Astrophys. J., 2-165 keV observations Act. galaxies diffuse Backgr.* 269, 423–437. doi:10.1086/161053

Rybicki, G. B., and Lightman, A. P. (1979). Radiative processes in astrophysics

Saade, M. L., Brightman, M., Stern, D., Malkan, M. A., and Garcia, J. A. (2022). NuSTAR observations of AGN with low observed X-ray to [OIII] luminosity ratios: heavily obscured AGN or turned-off AGN? *arXiv e-prints*. arXiv:2205.14216. doi:10.3847/1538-4357/ac88cf

Scepi, N., Begelman, M. C., and Dexter, J. (2021). Magnetic flux inversion in a peculiar changing look AGN. *Magnetic flux inversion a peculiar changing look AGN* 502, L50–L54. doi:10.1093/mnrasl/slab002

Schnittman, J. D., and Krolik, J. H. (2010). *Astrophys. J., X-ray Polariz. Accreting Black Holes Coronal Emiss.* 712, 908–924. doi:10.1088/0004-637X/712/2/908

Serafinelli, R., De Rosa, A., Tortosa, A., Stella, L., Vagnetti, F., Bianchi, S., et al. (2024). Investigating the interplay between the coronal properties and the hard X-ray variability of active galactic nuclei with NuSTAR. *A&* 690, A145. doi:10.1051/0004-6361/202450777

Shakura, N. I., and Sunyaev, R. A. (1973). Black holes in binary systems. Observational appearance. *A&A* 24, 337–355.

She, R., Ho, L. C., and Feng, H. (2017). Chandra survey of nearby galaxies: a significant population of candidate central black holes in late-type galaxies. *Galaxies* 842, 131. doi:10.3847/1538-4357/aa7634

Shemmer, O., Brandt, W. N., Netzer, H., Maiolino, R., and Kaspi, S. (2006). The hard X-ray spectral slope as an accretion rate indicator in radio-quiet active galactic nuclei. *ApJ* 646, L29–L32. doi:10.1086/506911

Shemmer, O., Brandt, W. N., Netzer, H., Maiolino, R., and Kaspi, S. (2008). The hard X-ray spectrum as a probe for black hole growth in radio-quiet active galactic nuclei. *Astrophys. J., Hard X-Ray Spectr. as a Probe Black Hole Growth Radio-Quiet Act. Galactic Nucl.* 682, 81–93. doi:10.1086/588776

Sironi, L., and Beloborodov, A. M. (2020). Kinetic simulations of radiative magnetic reconnection in the coronae of accreting black holes. *Astrophys. J., Kinet. Simulations Radiat. Magnetic Reconnect. Coronae Accreting Black Holes* 899, 52. doi:10.3847/1538-4357/aba622

Smith, J. F., and Courtier, G. M. (1976). The Ariel 5 programme. *Proc. R. Soc. Lond. Ser. A* 350, 421–439. doi:10.1098/rspa.1976.0115

Sobolewska, M. A., and Papadakis, I. E. (2009). The long-term X-ray spectral variability of AGN. *Mon. Not. R. Astron. Soc.* 399, 1597–1610. doi:10.1111/j.1365-2966.2009.15382.x

Sridhar, N., Ripperda, B., Sironi, L., Davelaar, J., and Beloborodov, A. M. (2024). Bulk motions in the black hole jet sheath as a candidate for the comptonizing corona. *arXiv e-prints*. arXiv:2411.10662doi. doi:10.48550/arXiv.2411.10662

Sridhar, N., Sironi, L., and Beloborodov, A. M. (2021). Comptonization by reconnection plasmoids in black hole coronae I: magnetically dominated pair plasma. *Mon. Not. R. Astron. Soc.* 507, 5625–5640. doi:10.1093/mnras/stab2534

Steffen, A. T., Strateva, I., Brandt, W. N., Alexander, D. M., Koekemoer, A. M., Lehmer, B. D., et al. (2006). The X-ray-to-optical properties of optically selected active galaxies over wide luminosity and redshift ranges. *aj* 131, 2826–2842. doi:10.1086/503627

Stern, B. E., Begelman, M. C., Sikora, M., and Svensson, R. (1995). A large-particle Monte Carlo code for simulating non-linear high-energy processes near compact objects. *Mon. Not. R. Astron. Soc.* 272, 291–307. doi:10.1093/mnras/272.2.291

Strateva, I. V., Brandt, W. N., Schneider, D. P., Vanden Berk, D. G., and Vignali, C. (2005). Soft X-ray and ultraviolet emission relations in optically selected AGN samples. *aj* 130, 387–405. doi:10.1086/431247

Swank, J. H. (1999). The rossi X-ray timing explorer. *Nucl. Phys. B Proc. Suppl.* 69, 12–19. doi:10.1016/S0920-5632(98)00175-3

Tagliacozzo, D., Marinucci, A., Ursini, F., Matt, G., Bianchi, S., Baldini, L., et al. (2023). The geometry of the hot corona in MCG-05-23-16 constrained by X-ray polarimetry. *Mon. Not. R. Astron. Soc., geometry hot corona MCG-05-23-16 constrained by X-ray Polarim.* 525, 4735–4743. doi:10.1093/mnras/stad2627

Takahashi, H. R., Kudoh, T., Masada, Y., and Matsumoto, J. (2011). Scaling law of relativistic sweet-parker-type magnetic reconnection. *Astrophysical J.* 739, L53. doi:10.1088/2041-8205/739/2/l53

Tanaka, Y., Inoue, H., and Holt, S. S. (1994). The X-ray astronomy satellite ASCA. *PASJ* 46, L37–L41.

Tananbaum, H., Wardle, J. F. C., Zamorani, G., and Avni, Y. (1983). X-ray studies of quasars with the Einstein Observatory. III the 3CR sample. *III. 3CR sample* 268, 60–67. doi:10.1086/160929

Tashiro, M., Maejima, H., Toda, K., Kelley, R., Reichenthal, L., Hartz, L., et al. (2020). "Status of x-ray imaging and spectroscopy mission (XRISM)," *Space telescopes and instrumentation 2020: ultraviolet to gamma ray*. Editors J.-W. A. den Herder, S. Nikzad, and K. Nakazawa (Society of Photo-Optical Instrumentation Engineers (SPIE) Conference Series), 11444. doi:10.1117/12.2565812

Taylor, B. G., Andresen, R. D., Peacock, A., and Zobl, R. (1981). The EXOSAT mission. *SSRv* 30, 479–494. doi:10.1007/BF01246069

Tchekhovskoy, A., Narayan, R., and McKinney, J. C. (2011). Efficient generation of jets from magnetically arrested accretion on a rapidly spinning black hole. *Effic. generation jets magnetically arrested accretion a rapidly Spinn. black hole* 418, L79–L83. doi:10.1111/j.1745-3933.2011.01147.x

Tortosa, A., Bianchi, S., Marinucci, A., Matt, G., and Petrucci, P. O. (2018). A NuSTAR census of coronal parameters in Seyfert galaxies. *A&* 614, A37. doi:10.1051/0004-6361/201732382

Tortosa, A., Ricci, C., Tombesi, F., Ho, L. C., Du, P., Inayoshi, K., et al. (2022). The extreme properties of the nearby hyper-Eddington accreting active galactic nucleus in IRAS 04416+1215. *Mon. Not. R. Astron. Soc., extreme Prop. nearby Eddingt. accreting Act. galactic Nucl. IRAS 04416+1215* 509, 3599–3615. doi:10.1093/mnras/stab3152

Trakhtenbrot, B., Arcavi, I., MacLeod, C. L., Ricci, C., Kara, E., Graham, M. L., et al. (2019). 1ES 1927+654: an AGN caught changing look on a timescale of months. *Astrophys. J., 1ES 1927+654 An AGN Caught Changing Look a Timescale Mon.* 883, 94. doi:10.3847/1538-4357/ab39e4

Treister, E., Urry, C. M., and Virani, S. (2009). *Astrophys. J., Space Density Compt. Act. Galactic Nucl. X-Ray Backgr.* 696, 110–120. doi:10.1088/0004-637X/696/1/110

Turner, T. J., Reeves, J. N., Braito, V., Lobban, A., Kraemer, S., and Miller, L. (2018). A rapid occultation event in NGC 3227. *Mon. Not. R. Astron. Soc., A rapid occultation event NGC 3227* 481, 2470–2478. doi:10.1093/mnras/sty2447

Ueda, Y., Akiyama, M., Hasinger, G., Miyaji, T., and Watson, M. G. (2014). *Astrophys. J., Toward Stand. Popul. Synthesis Model. X-Ray Backgr. Evol. X-Ray Luminosity Absorpt. Funct. Act. Galactic Nucl. Incl. Compt. Populations* 786, 104. doi:10.1088/0004-637X/786/2/104

Ursini, F., Matt, G., Bianchi, S., Marinucci, A., Dovčiak, M., and Zhang, W. (2022a). Prospects for differentiating extended coronal geometries in AGNs with the *IXPE* mission. *Mon. Not. R. Astron. Soc., Prospects Differ. Ext. coronal geometries AGNs IXPE mission* 510, 3674–3687. doi:10.1093/mnras/stab3745

Ursini, F., Matt, G., Bianchi, S., Marinucci, A., Dovčiak, M., and Zhang, W. (2022b). Prospects for differentiating extended coronal geometries in AGNs with the *IXPE* mission. *Mon. Not. R. Astron. Soc., Prospects Differ. Ext. coronal geometries AGNs IXPE mission* 510, 3674–3687. doi:10.1093/mnras/stab3745

Uttley, P., Cackett, E. M., Fabian, A. C., Kara, E., and Wilkins, D. R. (2014). X-ray reverberation around accreting black holes. *AAPR* 22, 72. doi:10.1007/s00159-014-0072-0

Uttley, P., McHardy, I. M., and Vaughan, S. (2005a). Non-linear X-ray variability in X-ray binaries and active galaxies. *Mon. Not. R. Astron. Soc., Non-linear X-ray Var. X-ray Bin. Act. galaxies* 359, 345–362. doi:10.1111/j.1365-2966.2005.08886.x

Uttley, P., McHardy, I. M., and Vaughan, S. (2005b). Non-linear X-ray variability in X-ray binaries and active galaxies. *Mon. Not. R. Astron. Soc., Non-linear X-ray Var. X-ray Bin. Act. galaxies* 359, 345–362. doi:10.1111/j.1365-2966.2005.08886.x

Vaiana, G. S., and Rosner, R. (1978). Recent advances in coronal physics. *ARAA* 16, 393–428. doi:10.1146/annurev.aa.16.090178.002141

van der Klis, M. (1989). Quasi-periodic oscillations and noise in low-mass X-ray binaries. *ARAA* 27, 517–553. doi:10.1146/annurev.aa.27.090189.002505

Vasudevan, R. V., and Fabian, A. C. (2007). Piecing together the X-ray background: bolometric corrections for active galactic nuclei: bolometric corrections for AGN. *Mon. Not. R. Astron. Soc., Piecing together X-ray Backgr. bolometric Correct. Act. galactic Nucl.* 381, 1235–1251. doi:10.1111/j.1365-2966.2007.12328.x

Vaughan, S., Edelson, R., Warwick, R. S., and Uttley, P. (2003a). On characterizing the variability properties of X-ray light curves from active galaxies. *Mon. Not. R. Astron. Soc., Charact. Var. Prop. X-ray light curves Act. galaxies* 345, 1271–1284. doi:10.1046/j.1365-2966.2003.07042.x

Vaughan, S., Fabian, A. C., and Nandra, K. (2003b). X-ray continuum variability of MCG-6-30-15. *Mon. Not. R. Astron. Soc., X-ray continuum Var. MCG-6-30-15* 339, 1237–1255. doi:10.1046/j.1365-8711.2003.06285.x

Vaughan, S., Uttley, P., Pounds, K. A., Nandra, K., and Strohmayer, T. E. (2011). The rapid X-ray variability of NGC 4051: the rapid X-ray variability of NGC 4051. *Mon. Not. R. Astron. Soc., rapid X-ray Var. NGC 4051* 413, 2489–2499. doi:10.1111/j.1365-2966.2011.18319.x

Weisskopf, M. C., O'Dell, S. L., and van Speybroeck, L. P. (1996). "Advanced X-ray astrophysics facility (AXAF)," in *Multilayer and grazing incidence X-ray/EUV optics III. 2805 of Society of photo-optical instrumentation engineers (SPIE) conference series*. Editors R. B. Hoover, and A. B. Walker, 2–7. doi:10.1117/12.245079

Weisskopf, M. C., Soffitta, P., Baldini, L., Ramsey, B. D., O'Dell, S. L., Romani, R. W., et al. (2022). Imaging X-ray polarimetry explorer: prelaunch. *J. Astronomical Telesc. Instrum. Syst.* 8, 026002. doi:10.1117/1.JATIS.8.2.026002

Wilkins, D. R., and Fabian, A. C. (2011). Determination of the X-ray reflection emissivity profile of 1H 0707-495: the emissivity profile of 1H 0707-495. *Mon. Not. R. Astron. Soc., Determ. X-ray Reflect. emissivity profile 1H 0707-495* 414, 1269–1277. doi:10.1111/j.1365-2966.2011.18458.x

Wilkins, D. R., and Fabian, A. C. (2012). Understanding X-ray reflection emissivity profiles in AGN: locating the X-ray source: X-ray reflection emissivity profiles in AGN. *Mon. Not. R. Astron. Soc., Underst. X-ray Reflect. emissivity profiles AGN locating X-ray source* 424, 1284–1296. doi:10.1111/j.1365-2966.2012.21308.x

Wilkins, D. R., and Fabian, A. C. (2013). The origin of the lag spectra observed in AGN: reverberation and the propagation of X-ray source fluctuations. *Mon. Not. R. Astron. Soc., Orig. lag spectra observed AGN Reverberation Propag. X-ray source fluctuations* 430, 247–258. doi:10.1093/mnras/sts591

Wilkins, D. R., and Gallo, L. C. (2015a). Driving extreme variability: the evolving corona and evidence for jet launching in Markarian 335. *Mon. Not. R. Astron. Soc.* 449, 129–146. doi:10.1093/mnras/stv162

Wilkins, D. R., and Gallo, L. C. (2015b). Driving extreme variability: the evolving corona and evidence for jet launching in Markarian 335. *Mon. Not. R. Astron. Soc.* 449, 129–146. doi:10.1093/mnras/stv162

Wilkins, D. R., and Gallo, L. C. (2015c). The Comptonization of accretion disc X-ray emission: consequences for X-ray reflection and the geometry of AGN coronae. *Mon. Not. R. Astron. Soc., Compt. accretion disc X-ray Emiss. consequences X-ray Reflect. geometry AGN coronae* 448, 703–712. doi:10.1093/mnras/stu2524

Wilkins, D. R., Gallo, L. C., Costantini, E., Brandt, W. N., and Blandford, R. D. (2022). Acceleration and cooling of the corona during X-ray flares from the Seyfert galaxy I Zw 1. *Mon. Not. R. Astron. Soc., Accel. Cool. corona Dur. X-ray flares Seyfert galaxy I Zw 1* 512, 761–775. doi:10.1093/mnras/stac416

Wilkins, D. R., Kara, E., Fabian, A. C., and Gallo, L. C. (2014). Caught in the act: measuring the changes in the corona that cause the extreme variability of 1H 0707–495. *Mon. Not. R. Astron. Soc., Caught act Meas. changes corona that cause extreme Var. 1H 0707-495* 443, 2746–2756. doi:10.1093/mnras/stu1273

Winkler, C., Courvoisier, T. J. L., Di Cocco, G., Gehrels, N., Giménez, A., Grebenev, S., et al. (2003). The INTEGRAL mission. *A&* 411, L1–L6. doi:10.1051/0004-6361:20031288

Worrall, D. M., Giommi, P., Tananbaum, H., and Zamorani, G. (1987). X-ray studies of quasars with the Einstein Observatory. IV - X-ray dependence on radio emission. *IV. X-Ray Dependence Radio Emiss.* 313, 596. doi:10.1086/164999

Zhang, W., Dovčiak, M., and Bursa, M. (2019). Constraining the size of the corona with fully relativistic calculations of spectra of extended coronae. I. The Monte Carlo radiative transfer code. *Monte Carlo Radiat. Transf. Code* 875, 148. doi:10.3847/1538-4357/ab1261

Zhu, S. F., Brandt, W. N., Luo, B., Wu, J., Xue, Y. Q., and Yang, G. (2020). The L_X-L_{uv}-L_{radio} relation and corona-disc-jet connection in optically selected radio-loud quasars. 496, 245–268. doi:10.1093/mnras/staa1411

Zoghbi, A., Fabian, A. C., Reynolds, C. S., and Cackett, E. M. (2012). Relativistic iron K X-ray reverberation in NGC 4151: iron K reverberation in NGC 4151. *Mon. Not. R. Astron. Soc., Relativistic iron K X-ray reverberation NGC 4151* 422, 129–134. doi:10.1111/j.1365-2966.2012.20587.x

Zoghbi, A., Fabian, A. C., Uttley, P., Miniutti, G., Gallo, L. C., Reynolds, C. S., et al. (2010). Broad iron L line and X-ray reverberation in 1H0707-495. *Mon. Not. R. Astron. Soc., Broad iron L line X-ray reverberation 1H0707-495* 401, 2419–2432. doi:10.1111/j.1365-2966.2009.15816.x

Zou, M., Hakobyan, H., Mbarek, R., Ripperda, B., Bacchini, F., and Sironi, L. (2024). A new particle pusher with hadronic interactions for modeling multimessenger emission from compact objects. *arXiv e-prints*. doi:10.48550/arXiv.2410.22781